Since January 2020 Elsevier has created a COVID-19 resource centre with free information in English and Mandarin on the novel coronavirus COVID-19. The COVID-19 resource centre is hosted on Elsevier Connect, the company's public news and information website.

Environmental Pollution 284 (2021) 117153

Contents lists available at ScienceDirect

Environmental Pollution

journal homepage: www.elsevier.com/locate/envpol

Increased ozone pollution alongside reduced nitrogen dioxide concentrations during Vienna's first COVID-19 lockdown: Significance for air quality management☆

Marlon Brancher

WG Environmental Health, Department of Biomedical Sciences, University of Veterinary Medicine Vienna, Veterinärplatz 1, A-1210, Vienna, Austria

ARTICLE INFO

Article history:
Received 26 January 2021
Received in revised form
19 March 2021
Accepted 13 April 2021
Available online 15 April 2021

Keywords:
COVID-19 lockdown
Air quality data
Atmospheric composition
Meteorology
Machine learning

ABSTRACT

Background: Lockdowns amid the COVID-19 pandemic have offered a real-world opportunity to better understand air quality responses to previously unseen anthropogenic emission reductions.
Methods and main objective: This work examines the impact of Vienna's first lockdown on ground-level concentrations of nitrogen dioxide (NO_2), ozone (O_3) and total oxidant (O_x). The analysis runs over January to September 2020 and considers business as usual scenarios created with machine learning models to provide a baseline for robustly diagnosing lockdown-related air quality changes. Models were also developed to normalise the air pollutant time series, enabling facilitated intervention assessment.
Core findings: NO_2 concentrations were on average −20.1% [13.7−30.4%] lower during the lockdown. However, this benefit was offset by amplified O_3 pollution of +8.5% [3.7−11.0%] in the same period. The consistency in the direction of change indicates that the NO_2 reductions and O_3 increases were ubiquitous over Vienna. O_x concentrations increased slightly by +4.3% [1.8−6.4%], suggesting that a significant part of the drops in NO_2 was compensated by gains in O_3. Accordingly, 82% of lockdown days with lowered NO_2 were accompanied by 81% of days with amplified O_3. The recovery shapes of the pollutant concentrations were depicted and discussed. The business as usual-related outcomes were broadly consistent with the patterns outlined by the normalised time series. These findings allowed to argue further that the detected changes in air quality were of anthropogenic and not of meteorological reason. Pollutant changes on the machine learning baseline revealed that the impact of the lockdown on urban air quality were lower than the raw measurements show. Besides, measured traffic drops in major Austrian roads were more significant for light-duty than for heavy-duty vehicles. It was also noted that the use of mobility reports based on cell phone movement as activity data can overestimate the reduction of emissions for the road transport sector, particularly for heavy-duty vehicles. As heavy-duty vehicles can make up a large fraction of the fleet emissions of nitrogen oxides, the change in the volume of these vehicles on the roads may be the main driver to explain the change in NO_2 concentrations.
Interpretation and implications: A probable future with emissions of volatile organic compounds (VOCs) dropping slower than emissions of nitrogen oxides could risk worsened urban O_3 pollution under a VOC-limited photochemical regime. More holistic policies will be needed to achieve improved air quality levels across different regions and criteria pollutants.

1. Introduction

The outbreak of the Coronavirus Disease 2019 (COVID-19) pandemic created unprecedented societal impacts worldwide. To lessen the virus spread, governments announced drastic non-pharmaceutical measures collectively referred to as lockdowns. In most European countries, the first series of lockdowns were imposed in early spring 2020. The restrictions led to an unseen drop in mobility and economic activities with associated sector-dependent reductions of anthropogenic air emissions (Evangeliou et al., 2021; Forster et al., 2020; Guevara et al., 2021; Le Quéré et al., 2020). For instance, less road traffic in cities will decrease the emissions of nitrogen oxides ($NO_x \equiv NO + NO_2$), a by-product of incomplete combustion of fossil fuels. Given the sources and short

☆ This paper has been recommended for acceptance by Pavlos Kassomenos.
E-mail address: Marlon.Brancher@vetmeduni.ac.at.

https://doi.org/10.1016/j.envpol.2021.117153

atmospheric lifetime of NO_x (Laughner and Cohen, 2019), their ambient concentrations are often higher close to busy streets in populated urban centres. Guidelines and limit values are typically enforced for nitrogen dioxide (NO_2), making it a relevant pollutant to study the impact of COVID-19 lockdowns on air quality. However, quantifying the air quality response from emission changes as a result of particular events such as COVID-19 lockdowns is not trivial due to the multifaceted nature of the atmosphere, and NO_2 is one regulated air pollutant of many.

Ozone (O3) in the troposphere is a greenhouse gas, a potent oxidant, and a harmful air pollutant. As a secondary pollutant, O_3 is produced or destructed in complex photochemical reactions of CO, CH_4 and other volatile organic compounds (VOCs) in the presence of NO_x (Archibald et al., 2020; Monks et al., 2015; Sillman, 1999). These precursors have anthropogenic and natural sources (Lu et al., 2019). Entrainment of O_3 from the stratosphere can also influence the distribution of surface O_3 (Collins et al., 2003). A common feature of O_3 chemistry is the highly non-linear dependence on its precursors. Because this chemistry has parallels with the input of NO_x and VOCs, it opens prospects to develop emission reduction policies (Seinfeld and Pandis, 2006). It is generally specified that under environments where VOC/NO_x ratios are high (low NO_x), the regime is NO_x-limited. Consequently, more NO_x will result in more O_3. This regime is seen more often in rural and suburban areas. For low VOC/NO_x ratios (high NO_x), the regime is NO_x-saturated or VOC-limited. This is typically observed in urban areas, where more NO_x does not produce more O_3 but the contrary (Kroll et al., 2020). The phenomenon, termed titration, means that reducing NO_x reduces the amount of O_3 being destructed via reaction with NO, and this essentially increases O_3 (Monks et al., 2015). Titration is a root cause of the weekend effect (de Foy et al., 2020; Sicard et al., 2020b), with O_3 levels increasing on weekends resulting from less road traffic and associated NO_x emissions. This fundamental chemistry could thus clarify observed increases in urban O_3 during lockdowns. However, the magnitude and sign of the O_3 change are not that straightforward. Accordingly, previous studies have reported mainly gains in urban areas, but also declines and no distinguishable change in O_3 levels during lockdowns (Adams, 2020; Dantas et al., 2020; Grange et al., 2021; Keller et al., 2021; Lovri et al., 2021; Luo et al., 2020; Miyazaki et al., 2020; Ordóñez et al., 2020; Sicard et al., 2020a; Siciliano et al., 2020; Singh et al., 2020; Soni et al., 2021). Besides NOx levels, this conclusion hinges on additional physical and chemical processes, such as the origin, ageing, amount and reactivity of the VOCs sources, the influence of biogenic VOCs, long-range transport of O_3, oxidant levels, on top of local weather conditions (Archibald et al., 2020; Kroll et al., 2020; Monks et al., 2015; Sillman, 1999; Stohl and Kromp-Kolb, 1994; Targino et al., 2019).

Meteorological conditions and chemistry play a central role in dictating air quality levels. These factors can confound the quantification of pollutant changes during lockdowns. The influence of confounders has been acknowledged, but relatively fewer studies have included this issue in the analysis (Grange et al., 2021; Jephcote et al., 2021; Keller et al., 2021; Lovri et al., 2021; Venter et al., 2020). More research is needed to increase our knowledge of the impacts of COVID-19 lockdowns on air quality, particularly by dealing with confounders critically in this kind of analysis.

Based on an ensemble of methods linking measurements and modelling, this work demonstrates a thorough analysis of the impact of the first COVID-19 lockdown on the air quality in Vienna, Austria. The focus is on ambient NO_2 and O_3 at ground level. Also, $O_x \equiv NO_2 + O_3$ has been added to the analysis to gain insights into the atmospheric oxidative capacity during the lockdown. The analysis shows how air quality responded until the end of September 2020, thereby covering a more extended period than most previous studies.

This work has four specific objectives. *First*, changes in road transportation are explored based on three different datasets to better understand potential changes in air quality and to provide insights for mobility-based emission estimations. *Second*, the importance of taking meteorology into account for more reliable lockdown-related air quality changes is shown, particularly for the present case of an urban boundary layer. *Third*, to account for the influence of meteorological variability itself and other time features, machine learning models are built to produce business as usual (BAU) and normalised pollutant time series. *Fourth*, this work investigates the potential bias when air quality changes are directly quantified from the pollutant measurements.

2. Methods

2.1. Study setting

Cities are at the heart of air quality management. By 2050, about two-thirds of the world's population is projected to be living in urban areas (United Nations, 2019). Vienna, the capital of Austria, had a population of 1,991,191 as of January 2020. The city is divided into 23 districts over a total area of 414.9 km^2 of which 50% are green spaces and water bodies, 36% built-up areas and 14% traffic areas. The highest elevation is Hermannskogel (543 m) and the lowest Lobau (151 m). The city does not accommodate major industries, except for an oil refinery in the South-east (SE). The total length of streets is 2,833 km with 714,960 private motor vehicles (including 3,853 electric cars). With a length of almost 18 km, the Viennese SE Tangent (A23 *Südosttangente*) is the shortest highway in Austria, but the busiest. The modal split share in Vienna is 38%, 30%, 25% and 7% for public transport, walking, driving and cycling, respectively. The car ownership rate is 37 cars/100 inhabitants, the lowest of the Austrian provincial capital cities (Statistics Vienna, 2020).

2.2. Data consideration and key periods under scrutiny

This work was designed based on the immediacy and availability of data, implying that only publicly available datasets have been considered. The major attention period of the first COVID-19 lockdown in Austria was from March 16 to April 13, 2020, inclusively (Pollak et al., 2020). Hereafter the lockdown imposed in this period is referred to as LOCK-2020. The identical period in the past five years is referred to as HIST-2015-2019.

2.3. Road transport data

Changes in road transport were explored based on three mobility datasets. First, monthly average daily traffic (MADT) counts were obtained from the ASFINAG | *Autobahnen-und Schnellstraßen-Finanzierungs-Aktiengesellschaft*'s motorway and expressway network for January to September in 2019 and 2020. This network includes currently about 270 measuring locations over Austria based on overhead (ultrasonic and passive infrared sensors) and inductive-loop detectors (ASFINAG, 2021). MADT data representing the number of vehicles that travel past (in both directions) a measuring location on all weekdays (Monday–Sunday), including bank holidays, were selected. Percentage changes on 2019 MADT data were calculated for individual months and summarised by vehicle category for the city and national levels. Two vehicle categories were considered: heavy-duty vehicles (HDV) whose maximum authorised overall weight is more than 3,500 kg

and light-duty vehicles (LDV) whose weight is less than or equal to 3,500 kg. The HDV category includes buses, trucks and articulated vehicles. The LDV category embraces motorcycles, cars and delivery vans.

Second, Apple's movement data were retrieved (Apple, 2021). Apple data originated from navigation requests for directions in Apple Maps. These data represent daily changes in the volume of people driving, walking or taking public transit corresponding to a baseline (January 13, 2020). Apple data did not consider day of the week influences. Of the three categories, driving was selected for the analysis.

Third, Google's movement data were used (Google, 2021). Google data were provided in six categories of which one was of interest: transit stations. These data represent how daily visits or length of stay at different places like public transport hubs for transit stations change compared to seven baseline days. Google selected a baseline day as the median value during the five-week period from January 3 to February 6, 2020 for the corresponding day of the week.

2.4. Air quality measurements

The analysis was built on validated and up-to-date hourly measurements of O_3 and NO_2 from seventeen monitors deployed across Vienna for the period between 2015 and September 30, 2020. Of these monitors, sixteen measure NO_2 and five measure O_3. A third pollutant was included as $O_x \equiv NO_2 + O_3$. O_x levels were calculated for four monitors. Detailed information on the individual monitors and measurement methods can be found elsewhere (Umweltschutzabteilung der Stadt Wien, 2020). Briefly, chemiluminescence and ultraviolet absorption are the methods used for NO_2 and O_3 measurements, respectively. Municipal Department 22 (https://www.wien.gv.at/umwelt/luft/index.html) provided air quality data. Up-to-date air quality data are unvalidated and subject to revision. As an attempt to assure data quality, the up-to-date data were screened for issues. These included frequent missing values (more than 10%), long lengths of gaps (more than 24 data points), unrealistic high values appearing abruptly (manual inspection of the time series), negative measurements, and repetitive sequences of measurements (in chunks of more than 6 data points); however, no prominent issues have been identified in the up-to-date data used herein. Figs. S1-S3 breakdown the availability of measurements by pollutant and monitor.

The Viennese air quality network has been designed to capture different exposure conditions, representing varying degrees of urbanisation. It comprises monitors at urban and suburban locations (area type). These locations are subdivided into background, traffic and industrial (station type). A combination of area type and station type (e.g., urban traffic) is hereafter referred to as environment. The monitors comprise five environments: urban traffic, urban background, suburban traffic, suburban industrial and suburban background.

2.5. Meteorological measurements

Initially, seven surface meteorological stations from the National Oceanic and Atmospheric Administration Integrated Surface Database (NOAA/ISD, https://www.ncdc.noaa.gov/isd) were identified. The NOAA/ISD meteorological data were accessed using the worldmet R package (Carslaw, 2020). As for the air quality measurements, the period between 2015 and September 30, 2020 was considered. The temporal resolution of the meteorological data is hourly. After screen checks, four of those stations were kept. Three stations (known as Groß-Enzersdorf, Donaufeld and Mariabrunn) were eliminated because of data gaps over LOCK-2020. For the monitor located at Hermannskogel, co-located meteorological measurements (data made available by Municipal Department 22) were considered. This was due to its more isolated position (488 m high) and the absence of an adjacent station in the NOAA/ISD database. Finally, five stations were selected. Fig. 1 illustrates the positions of the five meteorological stations and the seventeen air quality monitors in Vienna.

A prerequisite for developing this work was to propose an easily generalisable methodological design. With this in mind, the following routinely available and directly measured surface variables were selected: wind speed w_s (m s^{-1}), wind direction w_d (°), air temperature T_{air} (°C), atmospheric pressure P_{atm} (mb) and relative humidity RH (%). These variables were measured at all five meteorological stations. Based on representativeness, a meteorological station was designated for each air quality monitor (Table S1), and the meteorological and air pollutant datasets were paired under a mutual time frame (Coordinated Universal Time was used).

2.6. Business as usual modelling

Business as usual (BAU) scenarios in the form of pollutant time series were created using the random forest machine learning algorithm (Breiman, 2001). A total of 25 random forest models were grown to explain hourly-averaged concentrations per pollutant per monitor. This was done by feeding into the algorithm the meteorological variables previously described, besides time features which act as proxies for emissions and seasonality. The latter comprised Unix date t_{trend} (the trend term), Julian day t_{jd}, day of week t_{week}, and hour of day t_{hour}. The models can be written in terms of their nine common explanatory variables as follows

$$\left[\overline{C}\right] \sim w_s + w_d + T_{air} + P_{atm} + RH + t_{trend} + t_{jd} + t_{week} + t_{hour}, \quad \text{Eq. 1}$$

where $[\overline{C}]$ is the hourly-averaged concentration of the air pollutant of interest. When developing the models, the subsequent hyper-parameters were kept constant: node splitting with three variables, minimum node size of five and 300 trees (Grange et al., 2018). A training-testing splitting proportion of 70:30 was used. Several tuning tests were conducted, but the overall performance was steady with respect to the hyper-parameters selection and splitting fraction. Missing values of w_s and pollutant concentrations were removed prior to training. The models were grown from January 1, 2015 to February 15, 2020. From February 16 to September 30, 2020, the models predicted air pollutant concentrations forced by the meteorological conditions that were actually measured during this period. This strategy was implemented to (*i*) investigate air quality changes prior to and long after LOCK-2020 and (*ii*) verify the models' predictive skill to reproduce the pollutant measurements from February 16 to February 29, 2020. This second step is referred to as the verification phase. The duration of the verification phase was devised considering that the first two COVID-19 cases in Austria had been confirmed on February 25, 2020 (Pollak et al., 2020). Therefore, it was assumed no significant perturbations in anthropogenic emissions during the verification phase. The analysis of the road traffic patterns has proved valuable to support this assumption. Subsequently, the model-specific mean bias, $MB = \frac{1}{n}\sum_{i=1}^{n} P_i - O_i$, for the verification phase was used to calibrate the predictions. In the MB equation, O_i is the i_{th} observed value and P_i is the i_{th} predicted value for a total of n data points.

As the models were developed based on historical data prior to LOCK-2020, they are blind concerning the drastic perturbations in

Fig. 1. Locations of the air quality monitors and meteorological stations used in this study. Outer line represents the boundary of Vienna and inner lines represent the city's districts. (For interpretation of the references to colour in this figure legend, the reader is referred to the Web version of this article)

emissions caused by the COVID-19 crisis. As such, this approach considers that (local) emission sources would have remained operating normally under the observed meteorology. In other words, it simulates what would have been expected in the absence of COVID-19. BAU-related results were expressed as concentration deltas (Δ): the difference between the measurements and the predictions.

The modelling was conducted using the rmweather R package (Grange et al., 2018; Grange and Carslaw, 2019), which has underlying it the ranger R package (Wright and Ziegler, 2017).

2.7. Intervention assessment

The intrinsic variability in air pollutant time series complicates the detection of interventions and trends. In order to detach the contribution of influencing factors on measured pollutant concentrations, a normalisation technique was used (Grange and Carslaw, 2019). In addition to work in a predictive mode (for pollutant concentration forecasting), random forest models can also be used to diminish the effect of the explanatory variables on the dependent variable [$\overline{C}$]. This is done through sampling and predicting. To this end, another 25 random forest models were grown per pollutant per monitor following the previously described procedure (**Sec. 2.6**). The only difference was that these models were developed from 2015 to September 30, 2020 so that the MB calibration was not applicable here. The explanatory variables, excluding t_{trend}, were randomly sampled with replacement 300 times from the whole dataset for every time step. A model then predicts [$\overline{C}$] based on these inputs and returns the 300 predictions for each time step (hourly basis). The mean of the predictions for each hour was computed, and this forms the normalised pollutant time series that can be used for further exploration.

2.8. Data analysis

Hourly air pollutant concentrations were used to estimate mean changes (absolute and relative percentage). Changes in air quality were calculated for pollutants and monitors individually and by performing aggregations. A left-centred 7-day moving average was applied to highlight prevalent trends (longer-term) by smoothing out potentially large day-to-day fluctuations (shorter-term). The Mann-Whitney *U* test, a non-parametric method for equality of population medians of two independent samples, was used at a significance level of 0.01. Data analysis was performed in R using the openair (Carslaw and Ropkins, 2012) and tidyverse (Wickham et al., 2019) packages.

3. Results and discussion

3.1. Road traffic patterns

The month-by-month analysis of the MADT data indicates that the maximum reduction in road transport of −43% was reached in April 2020 in Vienna. Broken down by vehicle category, drops of −44% in LDV and −21% in HDV counts were found (Fig. 2, left panel). At the Austrian level, a maximum reduction in MADT of about −57% was also found in April 2020, with drops of −61% in LDV and −25% in HDV counts. In February 2020, an increase in MADT counts of +1% was observed for Vienna, with a +2% increase in LDV and a −2% drop in HDV. For Austria in February 2020, a decline in MADT counts of −1% was detected, with −0.8% and −3% drops in LDV and HDV, respectively. Thus, road traffic in Austria and Vienna until February 2020 did not undergo significant disruptions

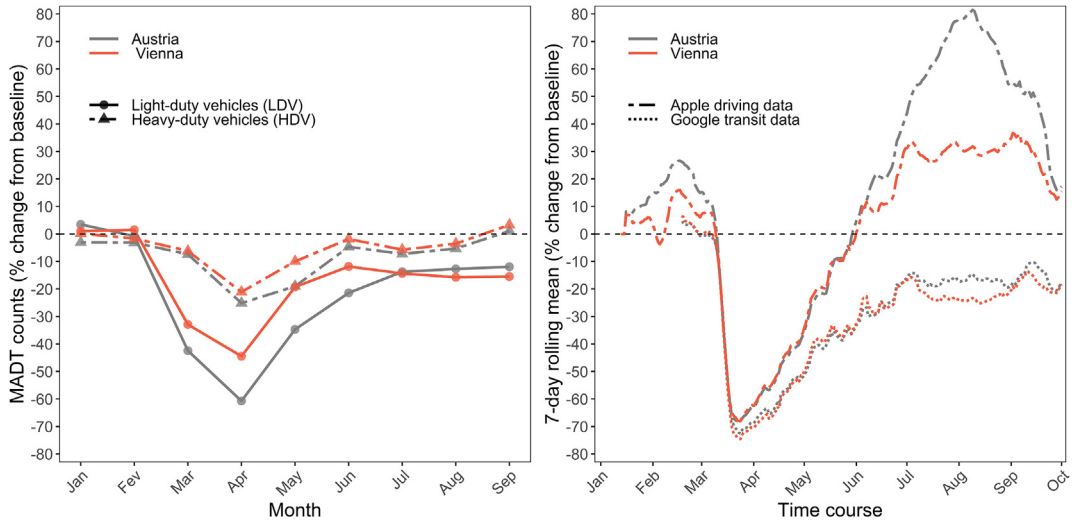

Fig. 2. Mobility changes (%) in the road transport sector for Vienna and Austria. *Left*: monthly-average daily traffic MADT counts for LDV and HDV. *Right*: 7-day rolling mean on the Google transit data and Apple driving data. See Methods for details on the baselines from which the percentage changes have been derived. (For interpretation of the references to colour in this figure legend, the reader is referred to the Web version of this article)

on major roads. These outcomes support calibrating the predictions of the BAU models based on the verification phase (February 16 to February 29, 2020). Furthermore, air traffic in Austrian airports showed akin trends to those of the road transport sector. An increase in passenger numbers of +7% was reported for February 2020, followed by drops of −65%, −100% and −99% in March, April and May 2020, respectively, compared with the same months in 2019 (STATISTIK AUSTRIA, 2020). Over the 9 months in 2020 (January–September 2020), MADT counts were down by −16% for Vienna and −21% for Austria relative to the same period in the previous year. These figures break down to −17% and −22% along with −5% and −8% drops in LDV and HDV counts for Vienna and Austria, respectively (Fig. 2, left panel). In view of these results, the Viennese MADT patterns were equivalent to those at the national level on major roads, but higher mean reductions in road traffic were generally observed for the country.

The changes in MADT counts also pinpoint that HDV were much less affected by the pandemic than LDV. This agrees with a previous study that has considered the same MADT metric for major roads in England (Jephcote et al., 2021). The difference between the two vehicles categories can be explained mainly because the HDV supported the shipment of goods and products during the lockdown (Guevara et al., 2021). After the peak in road traffic reductions in April 2020, a recovery in road traffic flows were observed in May and June 2020 for both vehicle categories. However, normal levels were not observed by the summer of 2020 compared with previous years' baseline. In particular for HDV, the levels were close to normal in June 2020 and were in fact found to occur first in September 2020 (Fig. 2, left panel).

Both Google transit and Apple driving data (Fig. 2, right panel) did not reflect well the HDV's activity on major Austrian roads over January–September 2020 (Fig. 2, left panel). Overall, the Google transit data appears to reflect the LDV's activity more closely. A similar outcome for a shorter period (2 months over February–April 2020) has been found for Spain/Barcelona (Guevara et al., 2021). Using Google transit data to estimate emission reductions, one assumes that mobility trends in public transport hubs can be taken as a proxy for trends in road traffic emissions (Guevara et al., 2021). Taken together, the present results support that this assumption is more appropriate for lighter vehicles than for heavier vehicles. Still, for both vehicle categories, the use of both Google transit and Apple driving data can pottentially overestimate the impact of the COVID-19 restrictions on road traffic emissions when compared with the changes in MADT counts. Dedicated studies will be required to resolve the identified issues to achieve improved emission estimates based on cell phone movement data. Anticipated gaps include differences in methodologies to derive the changes in mobility based on movement trends (e.g., different baseline periods) and representativeness of such trends. Here, Pearson's correlations (r) between the Apple driving data and Google transit data were 0.80 ($p < 0.01$) and 0.79 ($p < 0.01$) for Vienna and Austria, respectively. Such high correlations have also been noted during February–June 2020 for worldwide cities (Forster et al., 2020). However, it is clear from Fig. 2 (right panel) that there were marked divergences between Apple driving data with Google transit data over the summer months for both Vienna and Austria. The reason for this discrepancy is uncertain, but it may be that the Apple driving data is reflecting the behaviour of a particular type of travel pattern.

For the road traffic sector, emission reduction factors have been derived by using bottom-up approaches based on activity indicators such as cell phone movement data (Guevara et al., 2021; Menut et al., 2020). The problem of quantifying primary emissions as a result of COVID-19 lockdowns has serious implications for atmospheric modelling. The here-obtained insights by comparing mobility changes in road traffic using three distinct datasets have the potential to contribute to making progress in this regard.

3.2. Meteorological situation

Considering the meteorological situation is crucial to better understand air quality changes due to COVID-19 lockdowns. Accordingly, wind roses were produced for the LOCK-2020 and HIST-2015-2019 periods, besides the remaining data outside these periods from 2015 to September 30, 2020 (Fig. 3). Exposed are plots for the five selected meteorological stations, covering a good geographical area across Vienna. Wind roses were also produced for complete years in the 2015–2019 period (Fig. S4). First, there are some differences between the wind roses, which are due to the location of the stations. Vienna is mostly flat from South (S) to East (E) areas. However, the city is circumscribed from South-west (SW) to North-west (NW) by the moderate slopes of the Alpine foothills

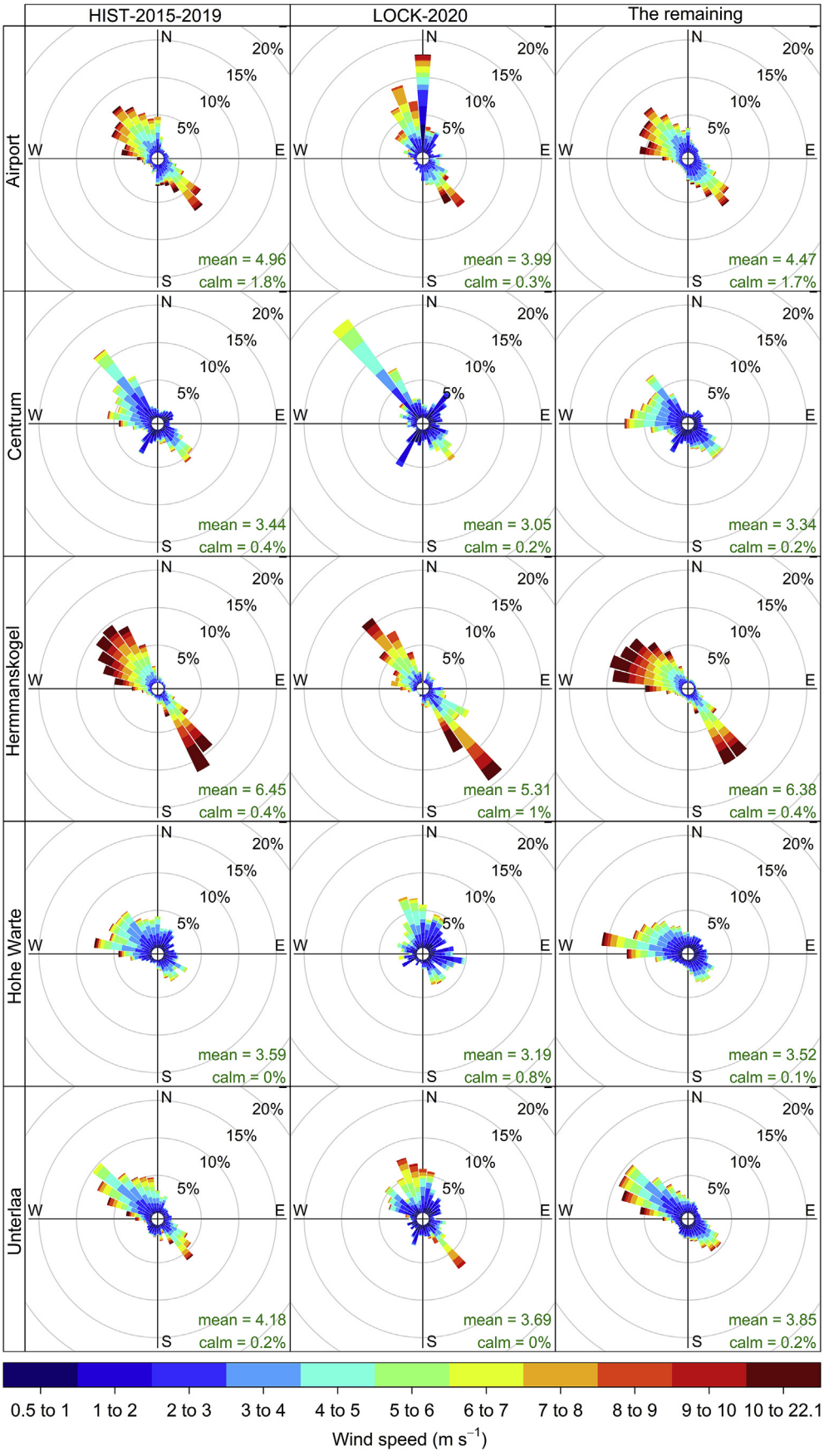

Fig. 3. Wind roses for the five selected meteorological stations and different periods (see text for the definition of the periods). The annotations in green show mean wind speeds and calm wind frequencies of each period. Calm winds were defined as having hourly speeds <0.5 m s^{-1}. The radial scale denotes the frequency of counts by wind direction sector. (For interpretation of the references to colour in this figure legend, the reader is referred to the Web version of this article)

(*Wienerwald*). Hence, the terrain becomes hilly at these parts, influencing the wind field. The longer-term wind roses demonstrate the city's typical airflow patterns. These are manifested by two dominant directions which are accompanied by higher speeds (Fig. 3, right panels and Fig. S4). The prevailing winds blow from West (W) to NW and from SE. The former has on average higher w_s than the latter. SE winds are more recurrently observed with fair weather (anticyclonic conditions). Contrary, W and NW winds are more connected to cloudy or rainy periods (Brancher et al., 2019a; 2019b). Moreover, SE winds on hilltops have a higher frequency than elsewhere, and there the highest w_s are observed. In the city centre, the w_s is reduced because of enhanced drag caused by a higher surface roughness length of the urban canopy layer. Also, not only T_{air} is increased (urban heat island), but RH (urban dry island) is typically reduced in the city centre.

Second, lower w_s were experienced for all five stations during LOCK-2020 relative to their preceding 5-year means for the same period, i.e. HIST-2015-2019. Alterations in w_d can be seen as well, such as more frequent flows from the North-northwest (NNW) and North (N) sectors (Fig. 3, central panels). The Austrian Weather Service (ZAMG) has reported a mild, sunny and mostly dry March 2020 in Austria. The reported T_{air}, precipitation and sunshine duration anomalies (1981–2010 climatology) were respectively +1.5 °C, −53% and +39% for Vienna. However, only the first two thirds of March 2020 were warmer than average. The LOCK-2020 period fits within the last third, and this was slightly colder due to the advance of polar cold air (ZAMG, 2020a). Furthermore, ZAMG has reported a truly warm, dry and sunny April 2020. The T_{air}, precipitation and sunshine duration anomalies were respectively +1.7 °C, −83% and +61% for Vienna. However, the cold front persisted until the first days of April 2020. The above-average T_{air} began from around April 5, 2020 (ZAMG, 2020b). When comparing LOCK-2020 against HIST-2015-2019 for the five selected stations, average differences of −0.7 °C, −0.7 m s^{-1} and +16% for T_{air}, w_s and RH were detected, respectively. This shows that whereas the LOCK-2020 period shares common features with March and April 2020, it had its own meteorological conditions.

Thus, care is called for when comparing identical lockdown periods. Even after reducing the variability by averaging over five previous years, the meteorological conditions between them can be dissimilar. It should be now straightforward to picture that meteorology is an exponentially growing issue for COVID-19 studies that have estimated air quality changes based on different lockdown periods.

3.3. Business as usual scenarios

3.3.1. Predictive performance

The random forest models' skill was evaluated for hourly data during the training/development phase (January 1, 2015–February 15, 2020) and verification phase (February 16—February 29, 2020). Tables S2—S4 dissects the performance summaries. The models were found to explain an adequate amount of the variation in the pollutant concentrations. For example, during the training/development phase, the models had *r* ranging from 0.82 to 0.91 for NO_2, from 0.93 to 0.95 for O_3, and from 0.95 to 0.96 for O_x. During the verification phase, there was a general reduction in performance, with the models showing *r* from 0.68–0.87 for NO_2, 0.54–0.82 for O_3, and 0.56–0.81 for O_x. Overall, the models' performance can be considered very satisfactory for hourly predictions, similar to up-to-date works (Font et al., 2020; Grange and Carslaw, 2019; Vu et al., 2019; Wang et al., 2020). Compared with deterministic, process-driven atmospheric chemistry models, the random forest models showed equivalent performance for the present application at a relatively lower computational cost (Menut et al., 2020).

It should be noted that the models struggled to reproduce the tails of the distributions. This is not a concern because herein mean air quality changes were examined, and the mean is known to be more robust than high or lower percentiles. Furthermore, the modelling workflow entails meteorological data. This work implemented a simple procedure to achieve models with adequate performance without the need for more sophisticated predictors. As such, the models are a good compromise between simplicity and predictive power. Instead of a long list of predictors, we paid more attention to selecting meteorological data with the potential to better describe smaller-scale air pollution variations in the urban area. Many studies select a 'regional' meteorological dataset (usually taken from a nearby airport station) to match air quality monitors in cities. The selection of representative surface meteorological stations is anticipated to be even more influential for complex terrain applications, as recently shown for a case in the Italian Alps (Falocchi et al., 2021).

The most important explanatory variables to predict hourly concentrations of NO_2, O_3 and O_x in Vienna were monitor dependent. On average, the importance for the NO_2 models was given in the following ascending order: w_s, w_d, t_{hour}, t_{jd}, T_{air}, RH, t_{week}, t_{trend} and P_{atm}; for the O_3 models as: RH, T_{air}, t_{jd}, w_s, t_{trend}, w_d, t_{hour}, P_{atm} and t_{week}; and for the O_x models in this manner: RH, T_{air}, t_{jd}, t_{trend}, w_s, w_d, t_{hour}, P_{atm} and t_{week}. The variables' importance agrees well with the chemical and physical processes expected to drive the dynamics of these pollutants (Jacob and Winner, 2009), thereby demonstrating the random forest models' interpretability nature. It is a universal observational feature that elevated O_3 concentrations are strongly correlated with T_{air} in polluted regions (Jacob and Winner, 2009). This is expected to be the case here too; however, the O_3 models suggest that RH is, on average, more important than T_{air}. Gaining insights into the processes that drive pollutant concentrations is crucial, particularly under a changing climate with regional differences (Von Schneidemesser et al., 2015). Consequently, these results on their own could be valuable to help better understand the sensitivity of O_3 pollution to meteorology in future studies.

3.3.2. Mean air quality changes

The NO_2 observations were consistently lower than the BAU predictions (Fig. 4). A mean decrease in NO_2 concentrations of −4.9 μg m^{-3} during the 29 days of LOCK-2020 was found at the city level. This equated to a mean percentage change of −20.1%. Keller et al. (2021) estimated monthly mean NO_2 changes for worldwide cities using machine learning (gradient boosting) coupled with the GEOS-CF model and mentioned some results for Vienna. They have reported drops in NO_2 concentrations in March and April 2020 of −20.6% and −26.2%, respectively. These monthly figures are not based on the specific lockdown period considered herein (LOCK-2020), but they align well with the present results.

NO_2 concentrations were reduced at all monitors, ranging from −1.4 to −12.7 μg m^{-3} or from −13.7 to 30.4%. The urban traffic Hietzinger Kai monitor showed the largest mean decrease (−12.7 μg m^{-3} or −30.4%) followed by other two urban traffic monitors, Gaudenzdorf (−7.2 μg m^{-3} or −22.8%) and A23-Wehlistraße (−7.0 μg m^{-3} or −21.8%). Across the network, the lowest NO_2 concentrations typically occur at Hermannskogel, a suburban background monitor located on the hilltop of a wooded area (Wienerwald). The mean reduction in NO_2 concentrations was −1.8 μg m^{-3} or −21.4% at Hermannskogel. This result shows that the drops in NO_x emissions from local sources in the urban core was strong enough to influence NO_2 concentrations at this monitor. Regarding NO_2 aggregations by environment, the influence of land use characteristics on the local spatial variations in NO_2

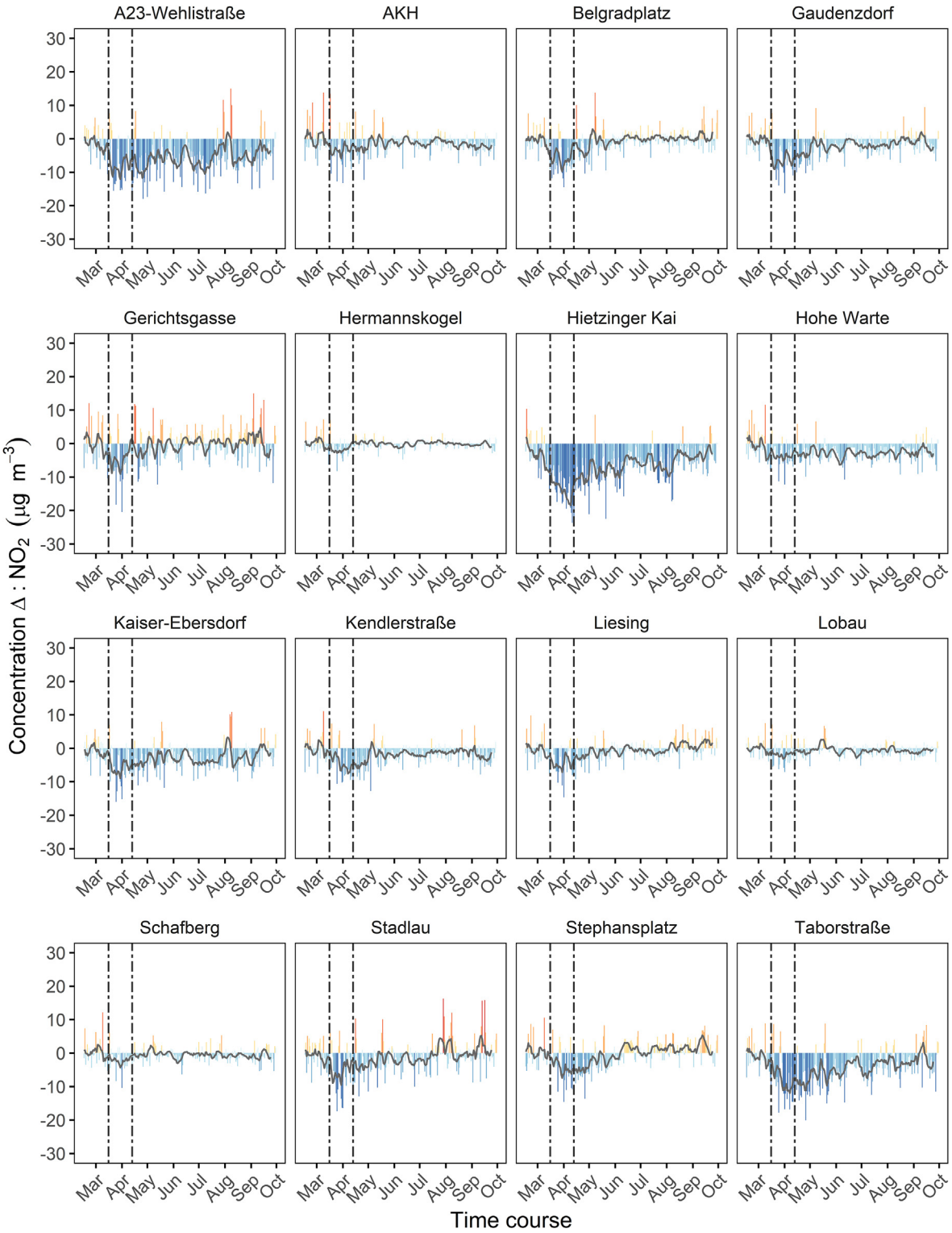

Fig. 4. Daily mean of NO_2 concentration deltas Δ. The study period runs between February 16 and September 30, 2020. The deltas represent the differences between the measured pollutant concentrations and the business as usual predictions. Solid grey lines are 7-day rolling means of the concentration deltas. Dashed vertical lines indicate the LOCK-2020 period.

concentrations has been detected. For instance, higher reductions in NO_2 concentrations were seen at urban traffic (-6.4 μg m^{-3} or -21.1%, $n = 8$) than at urban background (-4.1 μg m^{-3} or -18.5%, $n = 3$) and suburban background monitors (-1.7 μg m^{-3} or -15.9%, $n = 3$). These results were expected because of two main factors related to NO_2 pollution. First, NO_2 is a locally sensitive gas as it has a short atmospheric lifetime (Laughner and Cohen, 2019), meaning that it is not transported to regions far downwind of the emission sources. Second, NO_x emissions mainly come from fossil fuel combustion, especially in urban areas. Thus, NO_2 concentrations responded to declines in local NO_x emissions promptly as road transportation is the major emission source. By providing a quantitative assessment of the magnitude of this response, this work demonstrates how sensitive NO_2 pollution can be to future policy changes. To contextualise this point further, we can refer to the work of Grange et al. (2021). This work reported mean trends of NO_2 between 2010 and 2019 for major European urban areas of -1.44 μg m^{-3} y^{-1} at urban traffic and -0.72 μg m^{-3} y^{-1} at urban background environments. Assuming these concentration trends as a reference point for Vienna, the here-reported mean reductions due to the LOCK-2020 restrictions would indicate 4.4 and 5.7 years of sustained efforts to reduce NO_2 concentrations at those environments, respectively. For Hietzinger Kai, the mean reduction in NO_2 found during the lockdown would be equivalent to 8.8 years of continuous decline in ambient concentrations.

Negative daily NO_2 concentration Δ were found for 82% of the lockdown days. Two of the monitors (Hietzinger Kai and Gaudenzdorf) had only one day with positive daily NO_2 concentration Δ, stressing the clear signature of the COVID-19 pandemic on the NO_2 concentrations. The AKH monitor showed the lowest occurrence frequency of negative daily concentration Δ (69%) and one of the lowest reductions (-14.2%) in NO_2. This monitor is located nearby one of the largest hospitals in Europe, so it is reasonable to assume fewer reductions in road traffic around this hospital during LOCK-2020.

The largest departures of the NO_2 observed concentrations from the BAU forecasts generally occurred in early April 2020 (the exception was Hietzinger Kai, see Fig. 4). The return to normality (RTN) shapes of the NO_2 concentrations were more site-specific with some monitors recovering to BAU levels immediately after the lockdown (e.g., Hermannskogel, Lobau), in early May (e.g., Belgradplatz, Gaudenzdorf, Stephansplatz) or in late September 2020 (e.g., Hietzinger Kai, Hohe Warte). Altogether, the NO_2 RTN shapes, in particular at urban traffic environments, have strong similarities with the road transportation patterns shown in Fig. 2. In addition, decreases in NO_2 concentrations were found since early March 2020. This result indicates alterations in emissions effectively before LOCK-2020, which is again supported by the road traffic patterns for this period (**Sec. 3.1**). This is of significance for determining emission reduction factors in future studies. In follow-up research, it could also justify the definition of lockdown periods based on a statistical framework (Ropkins and Tate, 2021), contrary to static periods defined by official lockdown dates.

For O_3, the opposite behaviour to NO_2 has been found. There were clear increases in O_3 concentrations during LOCK-2020, as indicated by the observations being mostly greater than the counterfactual predictions during this period (Fig. 5). At the city level, O_3 concentrations increased by $+5.2$ μg m^{-3} or $+8.5\%$ on average. This relative change is greater than the monthly mean changes in March and April 2020 of respectively $+5.6\%$ and $+3.9\%$ given for Vienna (Keller et al., 2021). However, estimates of O_3 changes are very sensitive to the lockdown window (see Fig. 5).

O_3 pollution was amplified at all monitors, with gains ranging from $+2.1$–7.6 μg m^{-3} or $+3.7$–11.0%. In absolute terms, both the Hohe Warte and Hermannskogel monitors showed the largest increase of $+7.6$ μg m^{-3}. In relative terms, the largest increase of $+11.0\%$ occurred at Hohe Warte. The lowest increase occurred at Lobau, both in absolute and relative terms ($+2.1$ μg m^{-3} or $+3.6\%$). The mean change in O_3 concentrations during LOCK-2020 was slightly greater at urban background monitors ($+5.5$ μg m^{-3} or $+8.3\%$, $n = 3$) than at suburban background monitors ($+5.3$ μg m^{-3} or $+7.7\%$, $n = 2$). During the lockdown in the United Kingdom (UK) for instance, mean O_3 increases of $+7.2$ μg m^{-3} or 11% across the UK's urban background network have been reported (Lee et al., 2020).

The maximum occurrence frequency with daily O_3 concentrations above BAU levels was calculated for Hohe Warte (90% of the LOCK-2020 days). On average, positive daily O_3 concentration Δ were estimated for 81% of the days during the lockdown. By matching the monitors ($n = 4$) with concomitant NO_2 and O_3 observations, the occurrence frequency of negative and positive daily concentration Δ for NO_2 and O_3 were respectively 77% and 83% during the lockdown. In addition, whilst the NO_2 RTN shapes reflected the road traffic patterns (Fig. 2), the O_3 RTN shapes, in particular over the LOCK-2020 period, mirrored the NO_2 RTN shapes (direct comparisons can be made for Figs. 4 and 5 between the monitors where NO_2 and O_3 are measured concurrently).

Fig. 6 shows the O_x concentration Δ. It can be already grasped by visual inspection that the levels of O_x follow similar temporal patterns to those of O_3 (discussed further later). O_x concentrations increased by $+3.8$ μg m^{-3} at the city level during LOCK-2020, which equates to $+4.3\%$. The changes in O_x concentrations at urban background ($+4.3$ μg m^{-3} or $+5.2\%$, $n = 2$) were slightly greater than at suburban background monitors ($+3.4$ μg m^{-3} or $+4.1\%$, $n = 2$). Comparatively, the highest increase in O_x was seen at Hohe Warte ($+5.4$ μg m^{-3} or $+6.4\%$) and the smallest at Lobau ($+1.1$ μg m^{-3} or $+1.8\%$). All in all, lower NO_x and higher O_3 went side by side so that O_x levels increased only slightly.

After applying the Mann-Whitney *U* test, only two cases did not show statistically significant differences between the observations and BAU predictions. These were for O_3 and O_x at the Lobau monitor. All other pair of cases showed statistically significant differences ($p < 0.01$). Figs. S5–S7 depict the observations and BAU predictions themselves.

3.3.3. Further interpretation of the changes

To go further with the interpretation of the changes in air quality, Fig. 7 abridges the previously shown results by pollutant. The general impact of LOCK-2020 on the evaluated pollutants is depicted, besides their general RTN shapes over the study period. It is of interest first to contrast the mean NO_2 RTN shapes (Fig. 7, top panel) against Vienna's traffic patterns (Fig. 2, left panel). Mean NO_2 concentrations reached BAU levels during May 2020 for the first time. However, MADT counts for LDV were lower during the whole study period. MADT counts for HDV, which make up a smaller proportion of the vehicle fleet, did not fall so expressively, and almost normal levels were observed in June 2020 relative to the same month in 2019. This suggests the potential role played by HDV emissions to the surface NO_2 concentrations. Additional research will be required to understand this qualitative insight further; nevertheless, the present results are clear in noting the implications for air quality management. In this regard, a COVID-19-related study has emphasised that urban NO_x emissions are dominated by road traffic. However, this dominance could be much greater than currently reported in emission inventories (Lamprecht et al., 2021). Previous works also show that HDV dominate vehicular NO_x emissions (Ghaffarpasand et al., 2020; Song et al., 2018). Based on emission factors calculated from real-world observations of low-cost sensors, it has been shown that high emitters contribute disproportionately to fleet emissions of not only NO_x but also CO

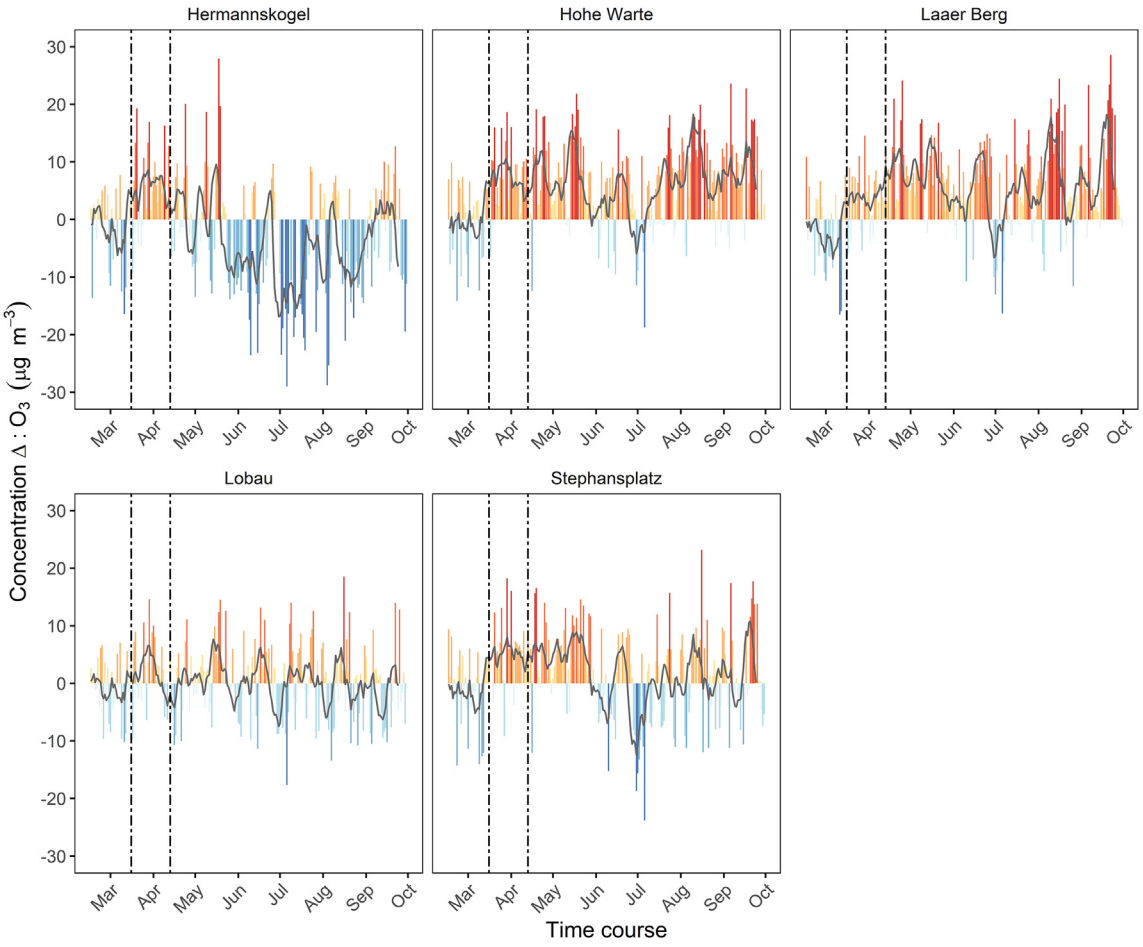

Fig. 5. Same as Fig. 4 but for O_3.

and $PM_{2.5}$ (Liu and Zimmerman, 2021). Similarly, by developing a city-level high-resolution vehicular emission inventory, Maes et al. (2019) reported that most NO_x emissions come from HDV. Hence, an important point to note here is that the changes in HDV counts could be the main driver of the changes in surface NO_2 concentrations during lockdowns. If so, control measures could be targeted at HDV with the potential to reduce total pollutant emissions from road traffic significantly and more effectively. It is recommended that such measures be integrated in the broader context of other emission sources and air pollutants. As the Viennese LOCK-2020 experience has shown for urban O_3, a key aspect of air quality management is to achieve a balanced strategy of emission reductions.

Moreover, the response of surface NO_2 to a change in NO_x emissions was estimated to have a mean sensitivity of 0.8 (Keller et al., 2021). This means that, on average, NO_2 concentrations at ground level reduce by roughly 80% of the fractional cut in anthropogenic NO_x emissions. A diminished effect was stated to occur for emission reductions larger than 50% because of atmospheric chemistry and background NO_2 influences (Keller et al., 2021).

Fig. 7 also illustrates the chemical coupling between O_3 and NO_2 and, in turn, O_x. During the whole study period (2015 to September 30, 2020), hourly O_x concentrations are driven mainly by O_3 ($r = 0.90$, $p < 0.01$). This positive correlation has not changed its strength during LOCK-2020.

It is essential to understand if the elevated concentrations of secondary pollutants like O_3 seen during strict lockdowns are due to chemistry (e.g., weakened titration, photochemical production and heterogeneous chemistry owing to decreased $PM_{2.5}$) or meteorological effects. As shown, the frequency of days with amplified O_3 concentrations was equivalent to the frequency of days with reduced NO_2 during the LOCK-2020 period in Vienna. After controlling for confounders, declines in NO_2 and gains in O_3 went hand in hand, so that O_x levels increased only slightly. This reflects a propensity of photochemical repartitioning of NO_2 to O_3, which is consistent with previous findings for European urban areas, and is not restricted to Vienna (Grange et al., 2021; Lee et al., 2020; Wyche et al., 2021). The present results therefore suggest the lower O_3 titration by NO as the dominant cause for explaining the O_3 increases in Vienna. In other words, the lockdown measures resulted in less ozone being depleted locally by NO due to the unprecedented reduction in NO_x emissions mainly from the road transport sector. Importantly, the outcome of gains in O_3 levels agrees with previous works for urban areas (Dantas et al., 2020; Grange et al., 2021; Le et al., 2020; Lee et al., 2020; Sicard et al., 2020a; Wyche et al., 2021).

The RO_2 (organic peroxy), OH (hydroxyl) and HO_2 (hydroperoxyl) radical species are central to tropospheric photochemistry (Levy, 1971; Monks et al., 2015; Seinfeld and Pandis, 2006; Sillman, 1999). The principal sources of these radicals in urban areas are the ultraviolet photolysis of O_3 itself, nitrous acid, and some carbonyls such as formaldehyde (Li et al., 2021 and references therein). The role of chlorine atoms as relevant tropospheric oxidants has been

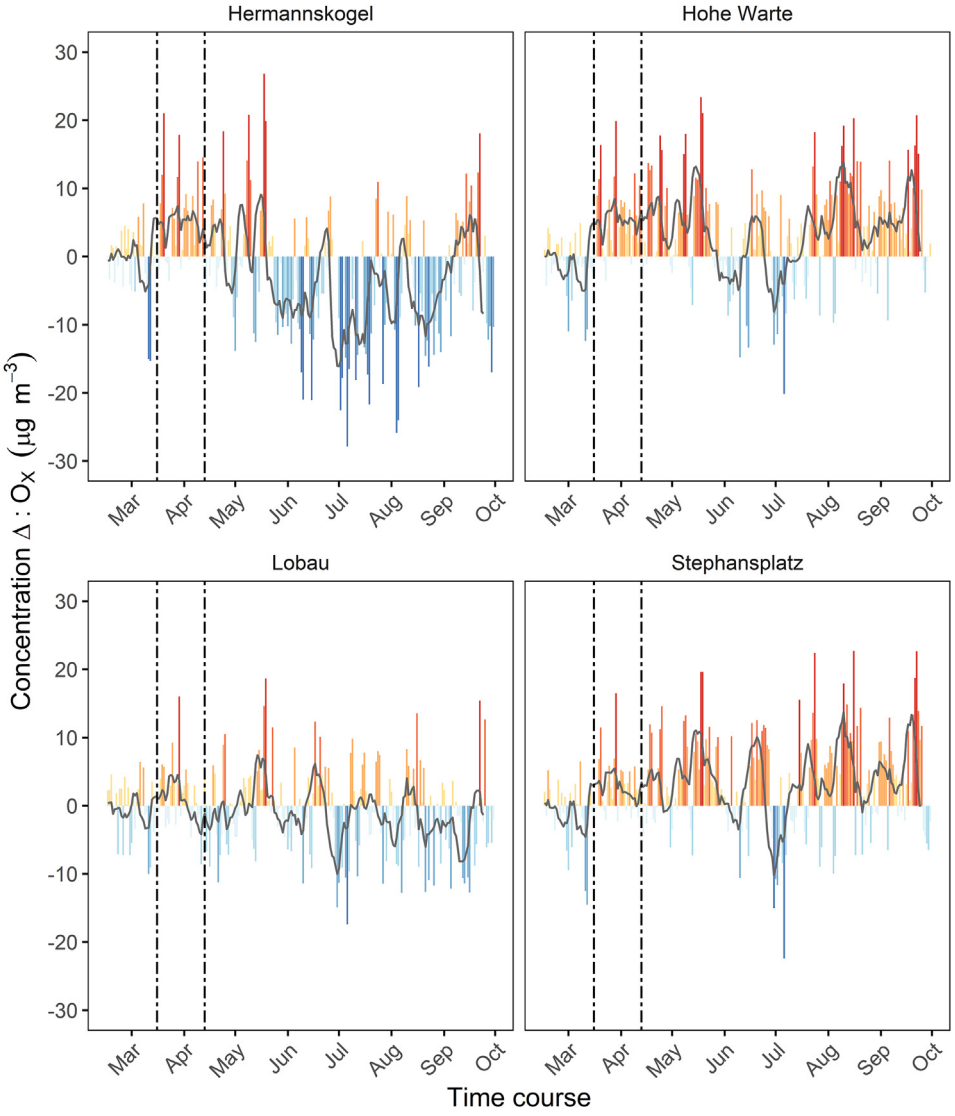

Fig. 6. Same as Fig. 4 but for O_x.

increasingly acknowledged too (Sommariva et al., 2021). The OH radical is particularly important because it initiates the removal of primary emissions, forming peroxy radicals (HO_2 and RO_2). Then, peroxy radicals form, in the presence of NO, secondary pollutants such as NO_2, O_3 and particulates (Whalley et al., 2021). If O_x remains preserved, the reduction of fresh NO emissions will increase O_3 concentrations because a lesser amount of O_x consists of NO_2 (Clapp and Jenkin, 2001). In this sense, changes in O_x can be understood as changes in the abundance of oxidants (Lee et al., 2020). As a consequence, the slight mean O_x increase during LOCK-2020 points to net photochemical production, which means that some part of the increase in O_3 is not solely attributable to weakened titration. It is premature to remark on the change in radical species without measurements or model calculations. However, as O_x is frequently used as an indicator of the atmospheric oxidative capacity (Chen et al., 2020; Grange et al., 2021), its small positive mean change is also suggesting some increase in overall reactivity of the urban boundary layer during LOCK-2020. With validated emission inventories, this premise can be tested with atmospheric chemistry models. For example, for China/Yangtze River Delta, a model study has reasoned that the dramatic reductions in NO_x during the lockdown were responsible for gains of the OH, HO_2 and NO_3 reactive radical species (Wang et al., 2021). Similarly, model simulations for the South East of the UK suggested increased radical levels, and indicated that the dominance of radical cycling over termination routes increased as a result of the lockdown (Wyche et al., 2021).

Regarding heterogeneous pathways, it has been suggested based on model simulations that the $PM_{2.5}$ decrease in the North China Plain since 2013 is the main driver for the O_3 increase due to reduced scavenging of HO_2 radicals to aerosol surfaces (Li et al., 2019). There is though continued debated from field studies on the general validity of the proposed mechanism (Tan et al., 2020). In order to make a simple comparison for Vienna, additional measurements were also taken for fine inhalable particles ($PM_{2.5}$). Directly from the observations, $PM_{2.5}$ decreased by -10.0% or -1.7 µg m^{-3} on average during LOCK-2020 compared with the same period in 2019. However, the finding by Li et al. is largely restricted to summer when $PM_{2.5}$ and O_3 had an overall positive correlation (Li et al., 2019, 2021). Observational data also showed that daily $PM_{2.5}$ and O_3 were negative correlated ($r = -0.34$, $p < 0.01$) during the LOCK-2020 period in Vienna. Thus, it is conjectured that this heterogenous

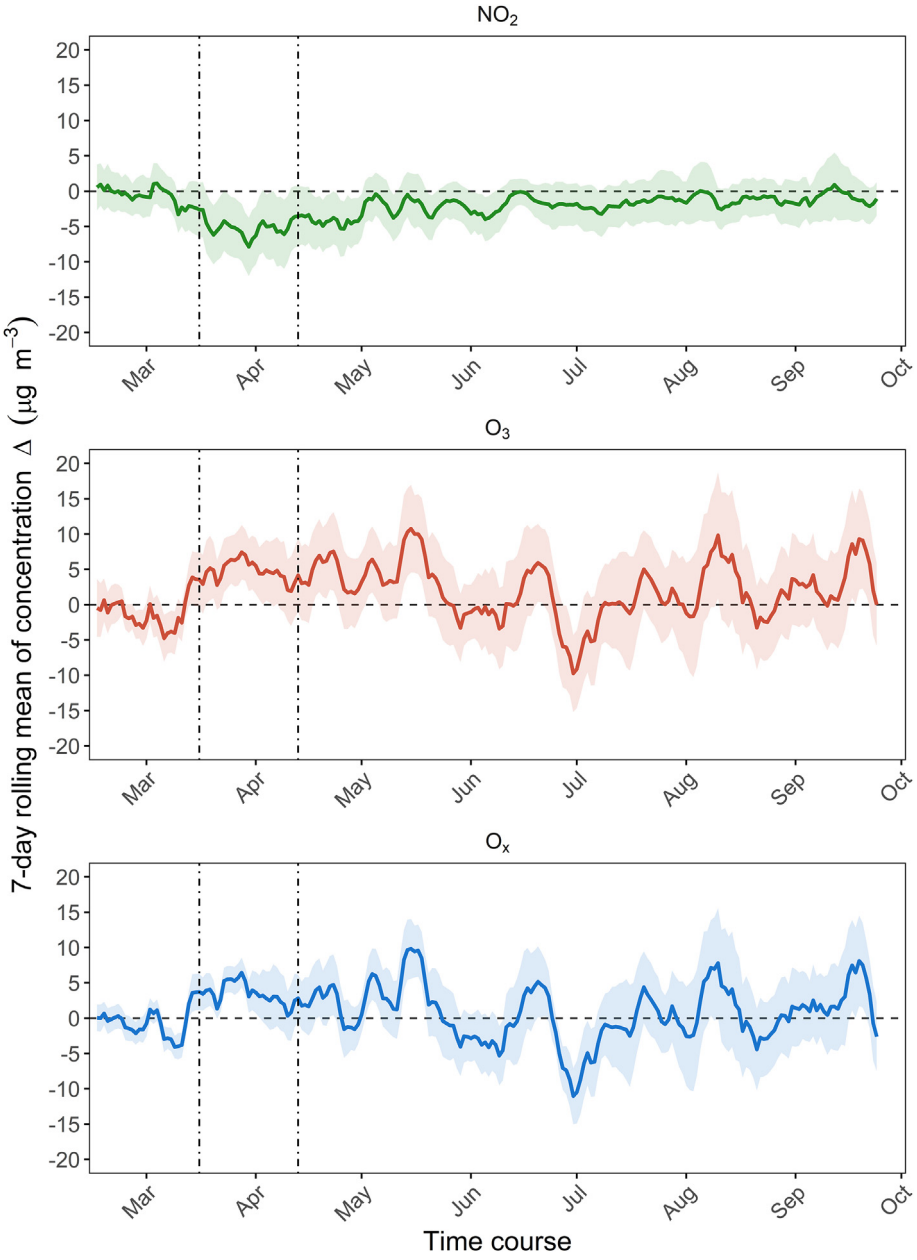

Fig. 7. Seven-day rolling mean of concentration deltas Δ for each pollutant between February 16 and September 30, 2020. Shaded areas are the standard deviation of the means. Dashed vertical lines indicate the LOCK-2020 period.

chemical pathway cannot explain the increases in O_3 during the lockdown. Despite such apparent mean decrease in $PM_{2.5}$ mass concentrations, a resultant oxidising environment may have facilitated secondary formation processes so that certain secondary aerosol components could show no changes or even increases (Sun et al., 2020).

Atmospheric chemistry models can separate local factors and regional transport to elucidate locally observed O_3 levels. It is acknowledged that the methods used here cannot rule out a potential contribution of regional transport of O_3. By assuming $PM_{2.5}$ a marker for transported pollution, we can make an educated guess of the potential influence of regional O_3 at the site location (Wyche et al., 2021). By comparing the daily mean concentrations of O_3 with $PM_{2.5}$ (not shown), correlated peaks in daily O_3 with respect to $PM_{2.5}$ were not detected during LOCK-2020 at two of the monitors with concomitant measurements of these pollutants (Lobau and Laaer Berg). As seen, a negative correlation between daily O_3 and $PM_{2.5}$ was calculated during the lockdown. This suggests that the increases in O_3 concentrations cannot merely be explained by transported pollution. Furthermore, according to Wyche et al. (2021), the existence of isolated peaks in the time series of daily O_3 concentration Δ indicates substantial contributions to local O_3 concentrations due to lockdown-induced perturbations in the O_3—NO_x—VOC boundary layer chemistry.

3.4. Normalised pollutant time series

Assessing the impact of interventions on air quality can be difficult for several reasons. The most problematic of these is perhaps meteorology. Meteorological effects can hide or even

accentuate the underlying changes in pollutant concentrations actually coming from perturbations in chemistry and emissions. Controlling for meteorology and other effects such as seasonality is thus essential when examining interventions on the basis of changes in air pollutant concentrations over time. Doing so allows intervention assessment and trend analysis to be explored robustly (Falocchi et al., 2021; Font et al., 2020; Grange et al., 2018; Grange and Carslaw, 2019; Ma et al., 2021; Vu et al., 2019). Here the normalisation technique was applied for intervention assessment by considering LOCK-2020 as the intervention, so its timing is known. The technique's main idea is to use statistical models to reduce variability in the air quality time series.

Fig. 8 shows the normalised pollutant concentration time series derived from the monitor-specific random forest models developed specifically for this purpose (Sec. 2.7). The predictive skill of these models was highly consistent with the performance of the models grown for the BAU scenarios during the model training and development phase (Tables S2—S4). The main intention of this quantitative analysis was to substantiate the previous results qualitatively. The overall NO_2 trend is a more gradual decline in concentrations going into the LOCK-2020 period. The normalised NO_2 time series did not show localised changeability during LOCK-2020 as they have broadly similar patterns. In addition, the normalised time series captured the recovery of the NO_2 concentrations following LOCK-2020. This again indicates widespread changes in the city rather than isolated changes, which is related to the intervention's spatial scale. However, the magnitude of the decline in NO_2 concentrations depends on the monitors' environment, as expected. We see again that the most noticeable drops in NO_2 concentrations occurred at the urban traffic monitors (e.g., Hietzinger Kai, A23-Wehlistraße). In this sense, even with a significant intervention, this analysis also shows the challenge of clearly distinguishing changes when air pollutant concentrations are around background levels. The normalised O_3 time series were able to depict the increases in concentrations of this pollutant during LOCK-2020. The increases in O_3 concentrations were apparent at the urban background monitors after the lockdown began (Laaer Berg, Hohe Warte, Stephansplatz), while more subtle at the suburban background monitors (Hermannskogel and Lobau). Regarding O_x, the normalised time series remained practically constant throughout LOCK-2020, indicating that the O_x abundance was not altered expressively. Besides the environment of an air quality monitor, Fig. 8 demonstrates that the efficacy of the intervention assessment depends strongly on the air pollutant under scrutiny.

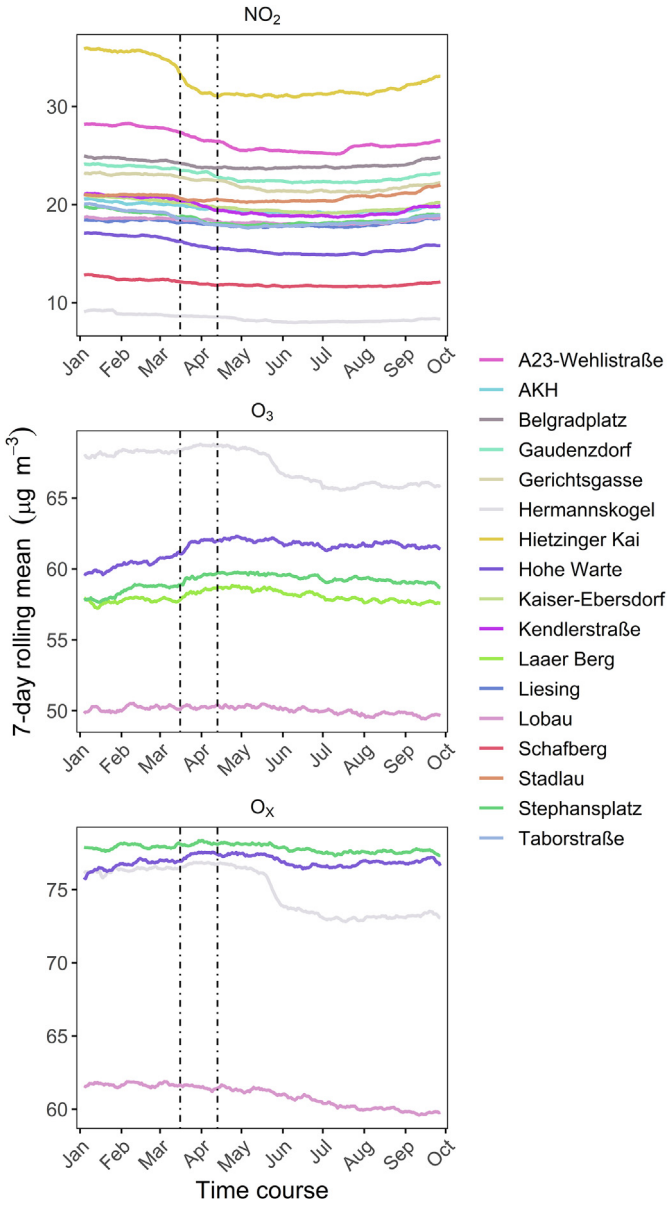

Fig. 8. Seven-day rolling mean of the normalised pollutant time series between January 1 and September 30, 2020. Dashed vertical lines indicate the LOCK-2020 period. (For interpretation of the references to colour in this figure legend, the reader is referred to the Web version of this article)

Collectively the results shown in Fig. 8 agree well with the BAU-related outcomes, adding a converging layer of evidence of how the first COVID-19 lockdown has impacted NO_2 and O_3 air pollution in Vienna. Besides, the normalised time series indicate further that the detected changes, or lack thereof, in the pollutant concentrations are of anthropogenic and not meteorological origin.

More generally, the suitability of the normalisation technique based on the random forest algorithm was shown for assessing the impact of a significant but relatively short-term intervention (Vienna's first COVID-19 lockdown) at the site location for different pollutants. This was achieved using existing, routine air quality monitoring and meteorological measurements. In light of contextual information, the normalisation technique facilitated explaining lockdown-associated characteristics in the pollutant time series to a great extent. These characteristics are not always evident in the raw data. It is also clear-cut from Fig. 8 that interventions taking place in a short period of time and on a small spatial scale could be very challenging to detect and quantify, or even go unnoticed, by using statistical approaches such as the normalisation technique applied in this work. This limitation should be considered for assessing the effectiveness of small spatio-temporal scale interventions. It could frustrate even those measurement programs carefully designed to collect data to feed the methods. Examples of policy interventions intentionally implemented to improve air pollution more locally include low emission zones, expansions of public transport service, fuel changes, traffic bans and modifications of bus routes.

3.5. The importance of accounting for confounders

A wide range of approaches has been applied to assess the impact of COVID-19 lockdowns on air quality (Grange et al., 2021; Hörmann et al., 2021; Krecl et al., 2020; Le et al., 2020; Ordóñez et al., 2020; Petetin et al., 2020; Ropkins and Tate, 2021; Sharma

et al., 2020; Tobías et al., 2020). This work contrasts a statistical approach (machine learning-based counterfactual predictions) against the 'historical approach'. The latter directly assesses air quality changes by comparing pollutant measurements during lockdowns with the same period in previous years. Due to its simplicity, it has been one of the most commonly used approaches. Here, the historical approach is based on the mean of the past five years (HIST-2015-2019) during the same period as the LOCK-2020.

The NO_2, O_3, and O_x changes on the random forest baseline reveal that the impact of Vienna's first COVID-19 lockdown on air quality was not as large as the raw pollutant measurements indicate (Fig. 9). Note that at the time of writing, a study also found that changes in pollutant concentrations due to lockdowns were more limited than previously reported (Shi et al., 2021). Bigger differences (up to a factor of ~2.3) between the two approaches were detected at the monitor scale compared with city-level aggregations. The present analysis further shows that the amount of bias differs not only by environment but also by pollutant. The bias is higher for O_3 and urban monitors. As shown in Sec. 3.2, a significant cause for the differences in the magnitude of changes stems from variations in meteorological conditions. Quantification of air quality changes relative to multi-year baseline values partially controls for the problem, but it cannot fully solve it (Venter et al., 2020). Moreover, meteorological conditions influence air pollutants differently. This goes back to the random forest models for NO_2 returning wind data as the most important explanatory variables. Similarly, the highest importance of the RH and T_{air} variables was given by the models developed for O_3 and O_x. Besides, potential pre-existing air pollutant trends due to reductions in primary emissions over the years also play a role in the historical approach. Hence, analyses of changes in air quality directly based on measured data resonate such confounding issues.

The direction of change was largely consistent between the two approaches, which holds for the LOCK-2020 duration (29 days). However, if shorter periods are considered, a previous study has shown that the historical approach can further exaggerate air quality changes (Petetin et al., 2020). This adds to the present results to conclude that the bias of the historical approach can increase at shorter temporal and finer spatial scales. In short, estimated changes in air quality from the historical approach should be interpreted with care for diurnal cycles at the site location.

3.6. Implications

Extensive epidemiological evidence shows the adverse health effects of exposure to air pollution (Cohen et al., 2017). Despite the dynamic interchange of NO_2 and O_3, relatively few studies have assessed the associations between health endpoints and exposure to these pollutants jointly. However, evidence is growing to indicate that the health effects of the simple sum of the two, $O_x \equiv NO_2 + O_3$, is greater than for either NO_2 or O_3 alone (Hvidtfeldt et al., 2019; Williams et al., 2014; Yang et al., 2016). This knowledge could lead to a growing interest in investigating and controlling O_x concentrations. Thus, the photochemical repartitioning of NO_2 to O_3 suggested by the first COVID-19 lockdown experience in Vienna may have consequences for public health and health impact assessments.

Successful management of O_3 pollution is challenging (Archibald et al., 2020; Monks et al., 2015). A central aspect of science-based policies is the O_3 formation regime (Wang et al., 2017). Conclusively stating the Viennese O_3 regime is hampered

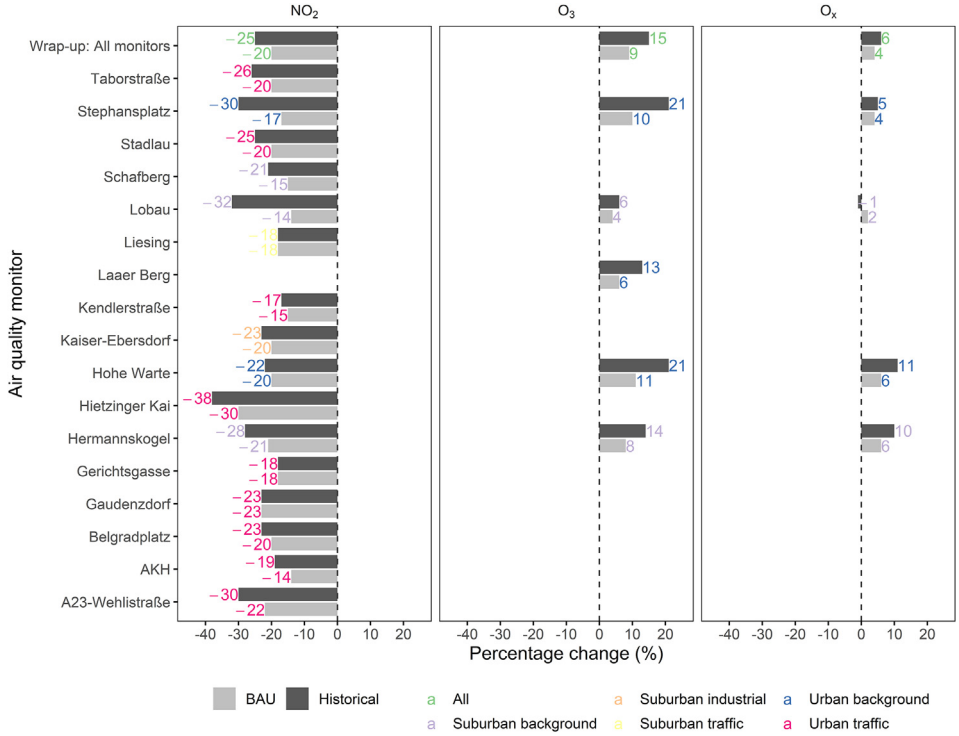

Fig. 9. Percentage changes in NO_2, O_3 and O_x from the machine learning-derived business as usual (BAU) scenarios against the historical approach (HIST-2015-2019). (For interpretation of the references to colour in this figure legend, the reader is referred to the Web version of this article)

because of the lack of routine VOC measurements concurrently with other pollutants. However, the present results indicate that the regime across Vienna is VOC-limited, which is typically seen for urban areas. Assuming that during the LOCK-2020 period, the supply of NO_x emissions reduced equivalently more than VOCs, this scenario would lead to higher VOC/NO_x ratios, resulting in an increase in O_3 pollution. This premise has been uncovered for example for Brazil/Rio de Janeiro: levels of O_3 increased more during the lockdown when air masses arrived at the monitors from industrial areas. This was due to the highest VOC/NO_x ratios and also the likely increase in reactivity of VOC mixtures rich in aromatic compounds (Siciliano et al., 2020). Fig. S8 shows the total anthropogenic NO_x and non-methane VOC emissions (NMVOC) from Austria's most recent inventory (Anderl et al., 2021) as well as the latest available projections to date in a scenario with existing measures (Anderl et al., 2019). If confirmed, projected total NMVOC emissions will exceed total NO_x emissions in the near future in Austria. The emission scenario associated with the first lockdown in Vienna gave us a clue of this probable future, signalling the risk of an increase in urban O_3. Therefore, to avoid potentially higher O_3 concentrations under these future projections, a control strategy should consider an equilibrium between the emission reductions of the different pollutants, especially focusing on heavier cuts in VOC emissions.

4. Conclusions

The present study focused on how NO_2 and O_3 air pollution responded to the strict government measures enforced in early spring 2020 to slow the spread of the SARS-CoV-2 virus in Vienna, Austria. Through an in-depth analysis of Vienna's first COVID-19 lockdown, this work shows that for a secondary pollutant like O_3, its mitigation will remain complex and challenging. A projected future with VOC emissions falling slower than NO_x emissions could risk an increase in urban ozone pollution under the VOC-limited conditions. Potential solutions include tailor-made, multi-pollutant strategies seeking to balance the emission reductions of O_3 precursors. In that sense, a recommendation is, in addition to reducing NO_x emissions, to instigate more aggresive cuts in VOC emissions. A deeper understanding of the effects posed by meteorology and chemistry when approached by scientific questions can be valuable so as to develop more efficacious policy responses.

We saw on the machine learning-based business as usual (BAU) baseline an improvement in air quality for NO_2 but not for O_3 during the LOCK-2020 period. The BAU scenarios showed that NO_2 concentrations reduced on average by −20.1% [13.7−30.4%] at the city level. However, O_3 concentrations increased by +8.5% [3.7−11.0%] across the city. O_x levels increased by +4.3% [1.8−6.4%], which is important in the context of repartitioning of NO_2 to O_3 and from a human health perspective. The slight increases in O_x levels also suggest an augmented oxidative capacity of the urban boundary layer owing to the imbalance in the reductions of primary anthropogenic emissions during LOCK-2020. The dominant cause of the increase in ambient O_3 during the lockdown was likely the lower O_3 titration by NO due to the large reductions in NO_x emissions. Accordingly, this works found that 82% of lockdown days with reduced ambient NO_2 concentrations were accompanied by 81% of days with increased O_3 pollution.

The recent access to global mobility data from big data providers offers a unique prospect for examining mobility changes from different standpoints. However, the use of Google transit data and Apple driving data can overestimate actual traffic reductions and associated emissions, especially for heavy-duty vehicles. Larger drops in road traffic volumes were observed for light-duty vehicles, while heavy-duty vehicles were much less affected by the COVID-19 pandemic. As heavy-duty vehicles are high NO_x emitters, the change in the volume of these vehicles on the roads may be the main driver behind the NO_2 reductions.

The impact of the lockdown on air quality was complex and significant, and its quantification is non-trivial. Nevertheless, this work suggests that air quality changes were probably not as large as previously reported. The present analysis demonstrated that accounting for confounders is crucial to appreciating air quality changes more robustly.

Credit author statement

Marlon Brancher: Conceptualisation, Methodology, Formal analysis, Investigation, Visualisation, Writing – original draft, Writing – review & editing, Project administration.

Declaration of competing interest

The author declares no known competing financial interests or personal relationships that could have appeared to influence the work reported in this paper.

Acknowledgements

Many thanks go to the institutions and professionals that provide open access datasets and tools, which have been essential to developing this work. Thanks to R. Plank (Stadt Wien | Umweltschutzabteilung MA 22) for furnishing the air quality data. Thanks to A. Fechner-Brancher for valuable discussions and proofreading the original manuscript. M. Brancher is currently supported by the Austrian Science Fund (FWF) in the framework of the Lise Meitner Programme [project number M 2548-N29].

Appendix A. Supplementary data

Supplementary data to this article can be found online at https://doi.org/10.1016/j.envpol.2021.117153.

References

Adams, M.D., 2020. Air pollution in ontario, Canada during the COVID-19 state of emergency. Sci. Total Environ. 742, 140516. https://doi.org/10.1016/j.scitotenv.2020.140516.

Anderl, M., Haider, S., Krutzler, T., Lampert, C., Poupa, S., Purzner, M., Schieder, W., Storch, A., Stranner, G., Titz, M., Zechmeister, A., 2019. Austria's national air emission projections 2019 for 2020, 2025 and 2030. Pollutants: NOx, SO2, NMVOC, NH3 and PM2.5. Scenario: with Existing Measures (WEM). In: REP-0689. Umweltbundesamt, Vienna.

Anderl, M., Haider, S., Lampert, C., Perl, D., Pinterits, M., Poupa, S., Purzner, M., Schieder, W., Schmidt, G., Schodl, B., Titz, M., Wieser, M., 2021. Austria's Annual Air Emission Inventory 1990—2019. Emissions of SO2 , NOx, NMVOC, NH3 and PM2,5. REP-0760. Umweltbundesamt, Vienna.

Apple, 2021. Mobility Trends Reports, 1.5.21. https://covid19.apple.com/mobility.

Archibald, A.T., Neu, J.L., Elshorbany, Y.F., Cooper, O.R., Young, P.J., Akiyoshi, H., Cox, R.A., Coyle, M., Derwent, R.G., Deushi, M., Finco, A., Frost, G.J., Galbally, I.E., Gerosa, G., Granier, C., Griffiths, P.T., Hossaini, R., Hu, L., Jöckel, P., Josse, B., Lin, M.Y., Mertens, M., Morgenstern, O., Naja, M., Naik, V., Oltmans, S., Plummer, D.A., Revell, L.E., Saiz-Lopez, A., Saxena, P., Shin, Y.M., Shahid, I., Shallcross, D., Tilmes, S., Trickl, T., Wallington, T.J., Wang, T., Worden, H.M., Zeng, G., 2020. Tropospheric Ozone Assessment Report: a critical review of changes in the tropospheric ozone burden and budget from 1850 to 2100. Elem. Sci. Anthr. 8 https://doi.org/10.1525/elementa.2020.034.

ASFINAG, 2021. Verkehrsentwicklung, 12.17.20. https://www.asfinag.at/verkehr/verkehrszaehlung/.

Brancher, M., Piringer, M., Franco, D., Belli Filho, P., De Melo Lisboa, H., Schauberger, G., 2019a. Assessing the inter-annual variability of separation distances around odour sources to protect the residents from odour annoyance. J. Environ. Sci. 79, 11−24. https://doi.org/10.1016/j.jes.2018.09.018.

Brancher, M., Piringer, M., Grauer, A.F., Schauberger, G., 2019b. Do odour impact criteria of different jurisdictions ensure analogous separation distances for an equivalent level of protection? J. Environ. Manag. 240, 394−403. https://doi.org/10.1016/j.jenvman.2019.03.102.

Breiman, L., 2001. Random forests. Mach. Learn. 45, 5–32. https://doi.org/10.1023/A:1010933404324.
Carslaw, D.C., 2020. Worldmet: import surface meteorological data from NOAA integrated surface database (ISD) [WWW Document]. URL. https://github.com/davidcarslaw/worldmet.
Carslaw, D.C., Ropkins, K., 2012. Openair — an R package for air quality data analysis. Environ. Model. Software 27 (28), 52–61. https://doi.org/10.1016/j.envsoft.2011.09.008.
Chen, S., Wang, H., Lu, K., Zeng, L., Hu, M., Zhang, Y., 2020. The trend of surface ozone in Beijing from 2013 to 2019: Indications of the persisting strong atmospheric oxidation capacity. Atmos. Environ. 242, 117801. https://doi.org/10.1016/j.atmosenv.2020.117801.
Clapp, L.J., Jenkin, M.E., 2001. Analysis of the relationship between ambient levels of O3 , NO2 and NO as a function of NOx in the UK. Atmos. Environ. 35, 6391–6405. https://doi.org/10.1016/S1352-2310(01)00378-8.
Cohen, A.J., Brauer, M., Burnett, R., Anderson, H.R., Frostad, J., Estep, K., Balakrishnan, K., Brunekreef, B., Dandona, L., Dandona, R., Feigin, V., Freedman, G., Hubbell, B., Jobling, A., Kan, H., Knibbs, L., Liu, Y., Martin, R., Morawska, L., Pope, C.A., Shin, H., Straif, K., Shaddick, G., Thomas, M., van Dingenen, R., van Donkelaar, A., Vos, T., Murray, C.J.L., Forouzanfar, M.H., 2017. Estimates and 25-year trends of the global burden of disease attributable to ambient air pollution: an analysis of data from the Global Burden of Diseases Study 2015. Lancet 389, 1907–1918. https://doi.org/10.1016/S0140-6736(17)30505-6.
Collins, W.J., Derwent, R.G., Garnier, B., Johnson, C.E., Sanderson, M.G., Stevenson, D.S., 2003. Effect of stratosphere-troposphere exchange on the future tropospheric ozone trend. J. Geophys. Res. Atmos. 108, 1–10. https://doi.org/10.1029/2002jd002617.
Dantas, G., Siciliano, B., França, B.B., da Silva, C.M., Arbilla, G., 2020. The impact of COVID-19 partial lockdown on the air quality of the city of Rio de Janeiro, Brazil. Sci. Total Environ. 729, 139085. https://doi.org/10.1016/j.scitotenv.2020.139085.
de Foy, B., Brune, W.H., Schauer, J.J., 2020. Changes in ozone photochemical regime in Fresno, California from 1994 to 2018 deduced from changes in the weekend effect. Environ. Pollut. 263, 114380. https://doi.org/10.1016/j.envpol.2020.114380.
Evangeliou, N., Platt, S.M., Eckhardt, S., Myhre, C.L., Laj, P., Alados-Arboledas, L., Backman, J., Brem, B.T., Fiebig, M., Flentje, H., Marinoni, A., Pandolfi, M., Yus-Dìez, J., Prats, N., Putaud, J.P., Sellegri, K., Sorribas, M., Eleftheriadis, K., Vratolis, S., Wiedensohler, A., Stohl, A., 2021. Changes in black carbon emissions over Europe due to COVID-19 lockdowns. Atmos. Chem. Phys. 21, 2675–2692. https://doi.org/10.5194/acp-21-2675-2021.
Falocchi, M., Zardi, D., Giovannini, L., 2021. Meteorological normalization of NO2 concentrations in the Province of Bolzano (Italian Alps). Atmos. Environ. 246, 118048. https://doi.org/10.1016/j.atmosenv.2020.118048.
Font, A., Tremper, A.H., Lin, C., Priestman, M., Marsh, D., Woods, M., Heal, M.R., Green, D.C., 2020. Air quality in enclosed railway stations: quantifying the impact of diesel trains through deployment of multi-site measurement and random forest modelling. Environ. Pollut. 262, 114284. https://doi.org/10.1016/j.envpol.2020.114284.
Forster, P.M., Forster, H.I., Evans, M.J., Gidden, M.J., Jones, C.D., Keller, C.A., Lamboll, R.D., Quéré, C. Le, Rogelj, J., Rosen, D., Schleussner, C.F., Richardson, T.B., Smith, C.J., Turnock, S.T., 2020. Current and future global climate impacts resulting from COVID-19. Nat. Clim. Change 10, 913–919. https://doi.org/10.1038/s41558-020-0883-0.
Ghaffarpasand, O., Beddows, D.C.S., Ropkins, K., Pope, F.D., 2020. Real-world assessment of vehicle air pollutant emissions subset by vehicle type, fuel and EURO class: New findings from the recent UK EDAR field campaigns, and implications for emissions restricted zones. Sci. Total Environ. 734, 139416. https://doi.org/10.1016/j.scitotenv.2020.139416.
Google, 2021. Community Mobility Reports, 1.5.21. https://www.google.com/covid19/mobility/.
Grange, S.K., Carslaw, D.C., 2019. Using meteorological normalisation to detect interventions in air quality time series. Sci. Total Environ. 653, 578–588. https://doi.org/10.1016/j.scitotenv.2018.10.344.
Grange, S.K., Carslaw, D.C., Lewis, A.C., Boleti, E., Hueglin, C., 2018. Random forest meteorological normalisation models for Swiss PM10 trend analysis. Atmos. Chem. Phys. 18, 6223–6239. https://doi.org/10.5194/acp-18-6223-2018.
Grange, S.K., Lee, J.D., Drysdale, W.S., Lewis, A.C., Hueglin, C., Emmenegger, L., Carslaw, D.C., 2021. COVID-19 lockdowns highlight a risk of increasing ozone pollution in European urban areas. Atmos. Chem. Phys. 21, 4169–4185. https://doi.org/10.5194/acp-21-4169-2021.
Guevara, M., Jorba, O., Soret, A., Petetin, H., Bowdalo, D., Serradell, K., Tena, C., Denier van der Gon, H., Kuenen, J., Peuch, V.-H., Pérez García-Pando, C., 2021. Time-resolved emission reductions for atmospheric chemistry modelling in Europe during the COVID-19 lockdowns. Atmos. Chem. Phys. 21, 773–797. https://doi.org/10.5194/acp-21-773-2021.
Hörmann, S., Jammoul, F., Kuenzer, T., Stadlober, E., 2021. Separating the impact of gradual lockdown measures on air pollutants from seasonal variability. Atmos. Pollut. Res. 12, 84–92. https://doi.org/10.1016/j.apr.2020.10.011.
Hvidtfeldt, U.A., Sørensen, M., Geels, C., Ketzel, M., Khan, J., Tjønneland, A., Overvad, K., Brandt, J., Raaschou-Nielsen, O., 2019. Long-term residential exposure to PM2.5, PM10, black carbon, NO2, and ozone and mortality in a Danish cohort. Environ. Int. 123, 265–272. https://doi.org/10.1016/j.envint.2018.12.010.
Jacob, D.J., Winner, D.A., 2009. Effect of climate change on air quality. Atmos. Environ. 43, 51–63. https://doi.org/10.1016/j.atmosenv.2008.09.051.
Jephcote, C., Hansell, A.L., Adams, K., Gulliver, J., 2021. Changes in air quality during COVID-19 'lockdown' in the United Kingdom. Environ. Pollut. 272, 116011. https://doi.org/10.1016/j.envpol.2020.116011.
Keller, C.A., Evans, M.J., Knowland, K.E., Hasenkopf, C.A., Modekurty, S., Lucchesi, R.A., Oda, T., Franca, B.B., Mandarino, F.C., Díaz Suárez, M.V., Ryan, R.G., Fakes, L.H., Pawson, S., 2021. Global impact of COVID-19 restrictions on the atmospheric concentrations of nitrogen dioxide and ozone. Atmos. Chem. Phys. 21, 3555–3592. https://doi.org/10.5194/acp-21-3555-2021.
Krecl, P., Targino, A.C., Oukawa, G.Y., Cassino Junior, R.P., 2020. Drop in urban air pollution from COVID-19 pandemic: Policy implications for the megacity of São Paulo. Environ. Pollut. 265, 114883. https://doi.org/10.1016/j.envpol.2020.114883.
Kroll, J.H., Heald, C.L., Cappa, C.D., Farmer, D.K., Fry, J.L., Murphy, J.G., Steiner, A.L., 2020. The complex chemical effects of COVID-19 shutdowns on air quality. Nat. Chem. 12, 777–779. https://doi.org/10.1038/s41557-020-0535-z.
Lamprecht, C., Graus, M., Striednig, M., Stichaner, M., Karl, T., 2021. Decoupling of urban CO2 and air pollutant emission reductions during the European SARS-CoV2 lockdown. Atmos. Chem. Phys. 21, 3091–3102. https://doi.org/10.5194/acp-21-3091-2021.
Laughner, J.L., Cohen, R.C., 2019. Direct observation of changing NOx lifetime in North American cities. Science 366, 723–727. https://doi.org/10.1126/science.aax6832.
Le Quéré, C., Jackson, R.B., Jones, M.W., Smith, A.J.P., Abernethy, S., Andrew, R.M., De-Gol, A.J., Willis, D.R., Shan, Y., Canadell, J.G., Friedlingstein, P., Creutzig, F., Peters, G.P., 2020. Temporary reduction in daily global CO2 emissions during the COVID-19 forced confinement. Nat. Clim. Change 10, 647–653. https://doi.org/10.1038/s41558-020-0797-x.
Le, T., Wang, Y., Liu, L., Yang, J., Yung, Y.L., Li, G., Seinfeld, J.H., 2020. Unexpected air pollution with marked emission reductions during the COVID-19 outbreak in China. Science 369, 702–706. https://doi.org/10.1126/science.abb7431.
Lee, J., Drysdale, W., Finch, D., Wilde, S., Palmer, P., 2020. UK surface NO2 levels dropped by 42 % during the COVID-19 lockdown: impact on surface O3. Atmos. Chem. Phys. 20, 15743–15759. https://doi.org/10.5194/acp-20-15743-2020.
Levy, H., 1971. Normal Atmosphere: Large Radical and Formaldehyde Concentrations Predicted. Science 173, 141–143. https://doi.org/10.1126/science.173.3992.141.
Li, K., Jacob, D.J., Liao, H., Qiu, Y., Shen, L., Zhai, S., Bates, K.H., Sulprizio, M.P., Song, S., Lu, X., Zhang, Q., Zheng, B., Zhang, Y., Zhang, J., Lee, H.C., Kuk, S.K., 2021. Ozone pollution in the North China Plain spreading into the late-winter haze season. Proc. Natl. Acad. Sci. U.S.A. 118, 1–7. https://doi.org/10.1073/pnas.2015797118.
Li, K., Jacob, D.J., Liao, H., Shen, L., Zhang, Q., Bates, K.H., 2019. Anthropogenic drivers of 2013–2017 trends in summer surface ozone in China. Proc. Natl. Acad. Sci. U.S.A. 116, 422–427. https://doi.org/10.1073/pnas.1812168116.
Liu, B., Zimmerman, N., 2021. Fleet-based vehicle emission factors using low-cost sensors: case study in parking garages. Transport. Res. Transport Environ. 91, 102635. https://doi.org/10.1016/j.trd.2020.102635.
Lovri, M., Pavlovi, K., Vukovi, M., Grange, S.K., Haberl, M., Kern, R., 2021. Understanding the true effects of the COVID-19 lockdown on air pollution by means of machine learning. Environ. Pollut. 115900. https://doi.org/10.1016/j.envpol.2020.115900.
Lu, X., Zhang, L., Shen, L., 2019. Meteorology and Climate Influences on Tropospheric Ozone: a Review of Natural Sources, Chemistry, and Transport Patterns. Curr. Pollut. Reports 5, 238–260. https://doi.org/10.1007/s40726-019-00118-3.
Luo, J., Qin, G., Cheng, J., 2020. Ozone pollution mitigation in guangxi (south China) driven by meteorology and anthropogenic emissions during the COVID-19. Environ. Pollut. https://doi.org/10.1016/j.envpol.2020.115927, 115927.
Ma, L., Graham, D.J., Stettler, M.E.J., 2021. Air quality impacts of new public transport provision: A causal analysis of the Jubilee Line Extension in London. Atmos. Environ. 245, 118025. https://doi.org/10.1016/j.atmosenv.2020.118025.
Maes, A. de S., Hoinaski, L., Meirelles, T.B., Carlson, R.C., 2019. A methodology for high resolution vehicular emissions inventories in metropolitan areas: Evaluating the effect of automotive technologies improvement. Transport. Res. Transport Environ. 77, 303–319. https://doi.org/10.1016/j.trd.2019.10.007.
Menut, L., Bessagnet, B., Siour, G., Mailler, S., Pennel, R., Cholakian, A., 2020. Impact of lockdown measures to combat Covid-19 on air quality over western Europe. Sci. Total Environ. 741, 140426. https://doi.org/10.1016/j.scitotenv.2020.140426.
Miyazaki, K., Bowman, K., Sekiya, T., Jiang, Z., Chen, X., Eskes, H., Ru, M., Zhang, Y., Shindell, D., 2020. Air quality response in China linked to the 2019 novel Coronavirus (COVID-19) lockdown. Geophys. Res. Lett. 47, 1–10. https://doi.org/10.1029/2020GL089252.
Monks, P.S., Archibald, A.T., Colette, A., Cooper, O., Coyle, M., Derwent, R., Fowler, D., Granier, C., Law, K.S., Mills, G.E., Stevenson, D.S., Tarasova, O., Thouret, V., Von Schneidemesser, E., Sommariva, R., Wild, O., Williams, M.L., 2015. Tropospheric ozone and its precursors from the urban to the global scale from air quality to short-lived climate forcer. Atmos. Chem. Phys. 15, 8889–8973. https://doi.org/10.5194/acp-15-8889-2015.
Ordóñez, C., Garrido-Perez, J.M., García-Herrera, R., 2020. Early spring near-surface ozone in Europe during the COVID-19 shutdown: Meteorological effects outweigh emission changes. Sci. Total Environ. 747, 141322. https://doi.org/10.1016/j.scitotenv.2020.141322.
Petetin, H., Bowdalo, D., Soret, A., Guevara, M., Jorba, O., Serradell, K., Pérez García-Pando, C., 2020. Meteorology-normalized impact of the COVID-19 lockdown upon NO2 pollution in Spain. Atmos. Chem. Phys. 20, 11119–11141. https://doi.org/10.5194/acp-20-11119-2020.

Pollak, M., Kowarz, N., Partheymüller, J., 2020. Chronology of the Corona Crisis in Austria - Part 1: Background, the Way to the Lockdown, the Acute Phase and Economic Consequences, 11.7.20. https://viecer.univie.ac.at/en/projects-and-cooperations/austrian-corona-panel-project/corona-blog/corona-blog-beitraege/blog51/.

Ropkins, K., Tate, J.E., 2021. Early observations on the impact of the COVID-19 lockdown on air quality trends across the UK. Sci. Total Environ. 754, 142374. https://doi.org/10.1016/j.scitotenv.2020.142374.

Seinfeld, J.H., Pandis, S.N., 2006. Atmospheric Chemistry and Physics from Air Pollution to Climate Change, 2 ed. Wiley, New Jersey.

Sharma, S., Zhang, M., Anshika Gao, J., Zhang, H., Kota, S.H., 2020. Effect of restricted emissions during COVID-19 on air quality in India. Sci. Total Environ. 728, 138878. https://doi.org/10.1016/j.scitotenv.2020.138878.

Shi, Z., Song, C., Liu, B., Lu, G., Xu, J., Van Vu, T., Elliott, R.J.R., Li, W., Bloss, W.J., Harrison, R.M., 2021. Abrupt but smaller than expected changes in surface air quality attributable to COVID-19 lockdowns. Sci. Adv. 7, eabd6696 https://doi.org/10.1126/sciadv.abd6696.

Sicard, P., De Marco, A., Agathokleous, E., Feng, Z., Xu, X., Paoletti, E., Rodriguez, J.J.D., Calatayud, V., 2020a. Amplified ozone pollution in cities during the COVID-19 lockdown. Sci. Total Environ. 735, 139542. https://doi.org/10.1016/j.scitotenv.2020.139542.

Sicard, P., Paoletti, E., Agathokleous, E., Araminienė, V., Proietti, C., Coulibaly, F., De Marco, A., 2020b. Ozone weekend effect in cities: Deep insights for urban air pollution control. Environ. Res. 191, 110193. https://doi.org/10.1016/j.envres.2020.110193.

Siciliano, B., Dantas, G., Cleyton, M., Arbilla, G., 2020. Increased ozone levels during the COVID-19 lockdown: Analysis for the city of Rio de Janeiro , Brazil. Sci. Total Environ. 737, 139765. https://doi.org/10.1016/j.scitotenv.2020.139765.

Sillman, S., 1999. The relation between ozone, NOx and hydrocarbons in urban and polluted rural environments. Atmos. Environ. 33, 1821–1845. https://doi.org/10.1016/S1352-2310(98)00345-8.

Singh, V., Singh, S., Biswal, A., Kesarkar, A.P., Mor, S., Ravindra, K., 2020. Diurnal and temporal changes in air pollution during COVID-19 strict lockdown over different regions of India. Environ. Pollut. 266, 115368. https://doi.org/10.1016/j.envpol.2020.115368.

Sommariva, R., Crilley, L.R., Ball, S.M., Cordell, R.L., Hollis, L.D.J., Bloss, W.J., Monks, P.S., 2021. Enhanced wintertime oxidation of VOCs via sustained radical sources in the urban atmosphere. Environ. Pollut. 274, 116563. https://doi.org/10.1016/j.envpol.2021.116563.

Song, C., Ma, C., Zhang, Y., Wang, T., Wu, L., Wang, P., Liu, Y., Li, Q., Zhang, J., Dai, Q., Zou, C., Sun, L., Mao, H., 2018. Heavy-duty diesel vehicles dominate vehicle emissions in a tunnel study in northern China. Sci. Total Environ. 637–638, 431–442. https://doi.org/10.1016/j.scitotenv.2018.04.387.

Soni, M., Ojha, N., Girach, I., 2021. Impact of COVID-19 lockdown on surface ozone build-up at an urban site in western India based on photochemical box modelling. Curr. Sci. 120, 376–381.

Statistics Vienna, 2020. Vienna in Figures 2020. Statistics, Vienna: Province of Vienna.

STATISTIK AUSTRIA, 2020. Wie hat sich der Flugbetrieb dieses Jahr verändert? Fluggäste auf Österreichs Flughäfen. In: Bundesanstalt Statistik Österreich. Zivilluftfahrtstatistik. 2020 Vorläufige Werte - Erstellt am 10.07.2020. https://www.statistik.at/. (Accessed 29 November 2020).

Stohl, A., Kromp-Kolb, H., 1994. Origin of ozone in Vienna and surroundings, Austria. Atmos. Environ. 28, 1255–1266. https://doi.org/10.1016/1352-2310(94)90272-0.

Sun, Y., Lei, L., Zhou, W., Chen, C., He, Y., Sun, J., Li, Z., Xu, W., Wang, Q., Ji, D., Fu, P., Wang, Z., Worsnop, D.R., 2020. A chemical cocktail during the COVID-19 outbreak in Beijing, China: Insights from six-year aerosol particle composition measurements during the Chinese New Year holiday. Sci. Total Environ. 742, 140739. https://doi.org/10.1016/j.scitotenv.2020.140739.

Tan, Z., Hofzumahaus, A., Lu, K., Brown, S.S., Holland, F., Huey, L.G., Kiendler-scharr, A., Li, X., Liu, X., Ma, N., Min, K., Rohrer, F., Shao, M., Wahner, A., Wang, Y., Wiedensohler, A., Wu, Y., Wu, Z., Zeng, L., Zhang, Y., Fuchs, H., 2020. No evidence for a significant impact of heterogeneous chemistry on radical concentrations in the North China plain in summer 2014. Environ. Sci. Technol. 54, 5973–5979. https://doi.org/10.1021/acs.est.0c00525.

Targino, A.C., Harrison, R.M., Krecl, P., Glantz, P., de Lima, C.H., Beddows, D., 2019. Surface ozone climatology of South Eastern Brazil and the impact of biomass burning events. J. Environ. Manag. 252, 109645. https://doi.org/10.1016/j.jenvman.2019.109645.

Tobías, A., Carnerero, C., Reche, C., Massagué, J., Via, M., Minguillón, M.C., Alastuey, A., Querol, X., 2020. Changes in air quality during the lockdown in Barcelona (Spain) one month into the SARS-CoV-2 epidemic. Sci. Total Environ. 726, 138540. https://doi.org/10.1016/j.scitotenv.2020.138540.

Umweltschutzabteilung der Stadt Wien, 2020. Jahresbericht 2019, Luftgütemessungen der Umweltschutzabteilung der Stadt Wien gemäß Immissionsschutzgesetz – Luft. MA 22 –376947/2020. Stadt Wien | Umweltschutz.

United Nations, 2019. World Urbanization Prospects: the 2018 Revision (ST/ESA/SER.A/420). Department of Economic and Social Affairs, Population Division, New York: United Nations.

Venter, Z.S., Aunan, K., Chowdhury, S., Lelieveld, J., 2020. COVID-19 lockdowns cause global air pollution declines. Proc. Natl. Acad. Sci. U.S.A. 117, 18984–18990. https://doi.org/10.1073/pnas.2006853117.

Von Schneidemesser, E., Monks, P.S., Allan, J.D., Bruhwiler, L., Forster, P., Fowler, D., Lauer, A., Morgan, W.T., Paasonen, P., Righi, M., Sindelarova, K., Sutton, M.A., 2015. Chemistry and the linkages between air quality and climate change. Chem. Rev. 115, 3856–3897. https://doi.org/10.1021/acs.chemrev.5b00089.

Vu, T.V., Shi, Z., Cheng, J., Zhang, Q., He, K., Wang, S., Harrison, R.M., 2019. Assessing the impact of clean air action plan on air quality trends in Beijing megacity using a machine learning technique. Atmos. Chem. Phys. 19, 11303–11314. https://doi.org/10.5194/acp-19-11303-2019.

Wang, T., Xue, L., Brimblecombe, P., Lam, Y.F., Li, L., Zhang, L., 2017. Ozone pollution in China: A review of concentrations, meteorological influences, chemical precursors, and effects. Sci. Total Environ. 575, 1582–1596. https://doi.org/10.1016/j.scitotenv.2016.10.081.

Wang, Y., Zhu, S., Ma, J., Shen, J., Wang, Pengfei, Wang, Peng, Zhang, H., 2021. Enhanced atmospheric oxidation capacity and associated ozone increases during COVID-19 lockdown in the Yangtze River Delta. Sci. Total Environ. 768, 144796. https://doi.org/10.1016/j.scitotenv.2020.144796.

Wang, Yunjie, Wen, Y., Wang, Yue, Zhang, S., Zhang, K.M., Zheng, H., Xing, J., Wu, Y., Hao, J., 2020. Four-month changes in air quality during and after the COVID-19 lockdown in six megacities in China. Environ. Sci. Technol. Lett. 7, 802–808. https://doi.org/10.1021/acs.estlett.0c00605.

Whalley, L.K., Slater, E.J., Woodward-Massey, R., Ye, C., Lee, J.D., Squires, F., Hopkins, J.R., Dunmore, R.E., Shaw, M., Hamilton, J.F., Lewis, A.C., Mehra, A., Worrall, S.D., Bacak, A., Bannan, T.J., Coe, H., Percival, C.J., Ouyang, B., Jones, R.L., Crilley, L.R., Kramer, L.J., Bloss, W.J., Vu, T., Kotthaus, S., Grimmond, S., Sun, Y., Xu, W., Yue, S., Ren, L., Acton, W.J.F., Hewitt, C.N., Wang, X., Fu, P., Heard, D.E., 2021. Evaluating the sensitivity of radical chemistry and ozone formation to ambient VOC_s and NO_x in Beijing. Atmos. Chem. Phys. 21, 2125–2147. https://doi.org/10.5194/acp-21-2125-2021.

Wickham, H., Averick, M., Bryan, J., Chang, W., McGowan, L., François, R., Grolemund, G., Hayes, A., Henry, L., Hester, J., Kuhn, M., Pedersen, T., Miller, E., Bache, S., Müller, K., Ooms, J., Robinson, D., Seidel, D., Spinu, V., Takahashi, K., Vaughan, D., Wilke, C., Woo, K., Yutani, H., 2019. Welcome to the tidyverse. J. Open Source Softw. 4, 1686. https://doi.org/10.21105/joss.01686.

Williams, M.L., Atkinson, R.W., Anderson, H.R., Kelly, F.J., 2014. Associations between daily mortality in London and combined oxidant capacity, ozone and nitrogen dioxide. Air Qual. Atmos. Heal. 7, 407–414. https://doi.org/10.1007/s11869-014-0249-8.

Wright, M.N., Ziegler, A., 2017. Ranger: a fast implementation of random forests for high dimensional data in C++ and R. J. Stat. Software 77, 1–17. https://doi.org/10.18637/jss.v077.i01.

Wyche, K.P., Nichols, M., Parfitt, H., Beckett, P., Gregg, D.J., Smallbone, K.L., Monks, P.S., 2021. Changes in ambient air quality and atmospheric composition and reactivity in the South East of the UK as a result of the COVID-19 lockdown. Sci. Total Environ. 755, 142526. https://doi.org/10.1016/j.scitotenv.2020.142526.

Yang, C., Li, H., Chen, R., Xu, W., Wang, C., Tse, L.A., Zhao, Z., Kan, H., 2016. Combined atmospheric oxidant capacity and increased levels of exhaled nitric oxide. Environ. Res. Lett. 11, 074014 https://doi.org/10.1088/1748-9326/11/7/074014.

ZAMG, 2020a. März 2020 mild, sonnig und größtenteils trocken, 11.25.20. https://www.zamg.ac.at/cms/de/klima/news/maerz-2020-mild-sonnig-und-groesstenteils-trocken.

ZAMG, 2020b. April 2020 sehr warm, sehr trocken und sehr sonnig, 11.25.20. https://www.zamg.ac.at/cms/de/klima/news/april-2020-sehr-warm-sehr-trocken-und-sehr-sonnig.